Analysis & Sensing

Review
doi.org/10.1002/anse.202200103

Chemistry Europe
European Chemical Societies Publishing

www.analysis-sensing.org

Lipid Analysis by Mass Spectrometry coupled with Laser Light

Carla Kirschbaum*[a, b] and Kevin Pagel[a, b]

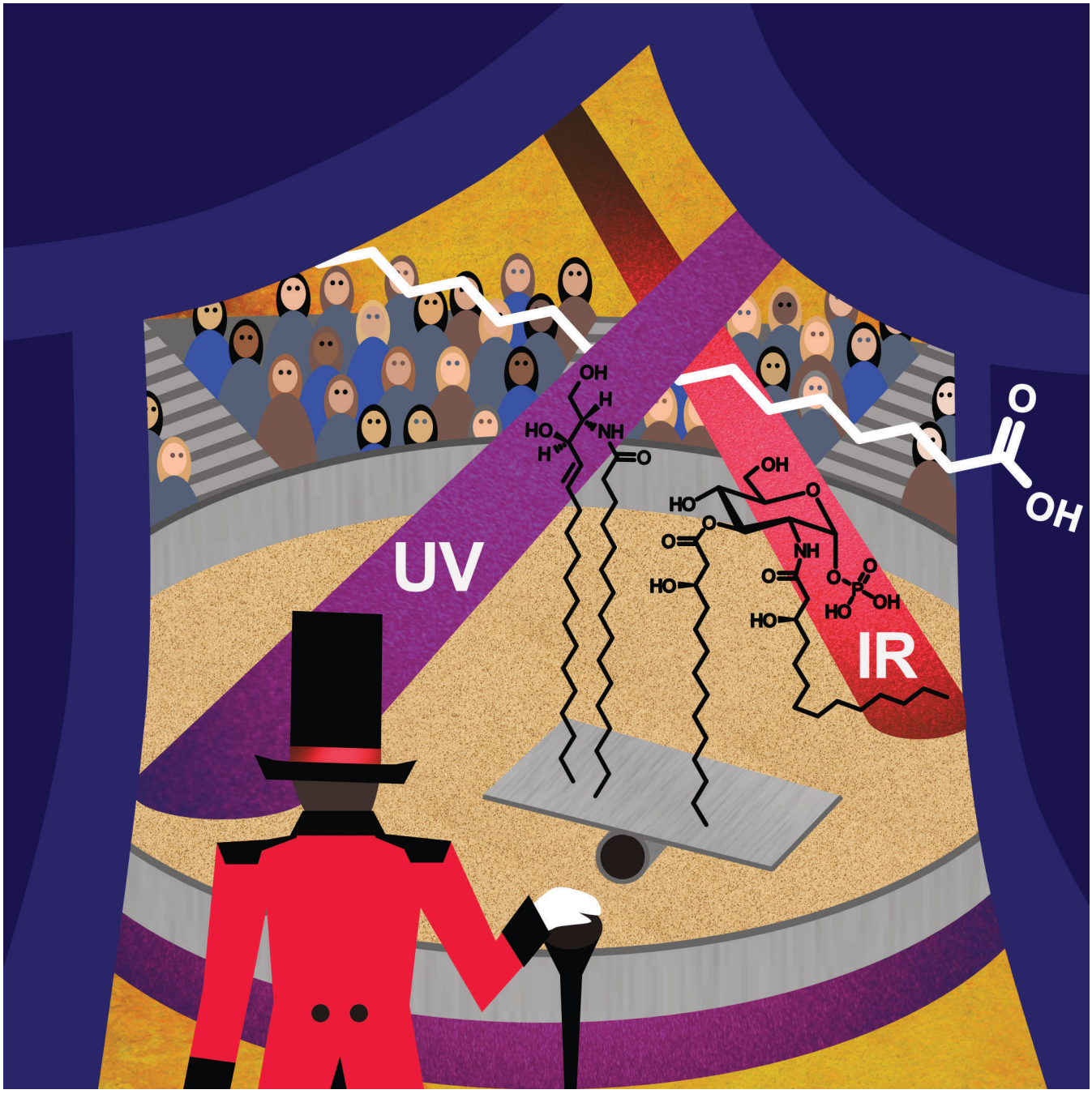

Lipids are small but complex biomolecules that feature an immense structural and functional diversity. The molecular structure and biological functions of lipids are intricately linked. Therefore, modern lipid analysis strives for complete structural elucidation and spatial mapping of individual species in tissues. Mass spectrometry is the uncontested key technology in lipidomics but cannot achieve this goal as a standalone technique. In particular, the distinction between frequently occurring isomers constitutes a major challenge. A promising step towards complete structural analysis of lipids consists in the coupling of mass spectrometry with laser light. Here we review recent advances in lipidomics applications employing laser-induced ultraviolet and infrared photodissociation and ion spectroscopy, which substantially increase the gain in structural information. Fundamental concepts, instrumentation and promises of these powerful emerging techniques for future lipid analysis are outlined.

1. Introduction

Lipids constitute a heterogeneous class of biomolecules that are involved in energy storage, signaling, modulation of membrane protein function and cell compartmentalization.[1] The multitude of biological functions is reflected in a tremendous structural diversity and coexistence of multiple isomers.[2] Due to the strong structure-function relationship, individual isomers can fulfill distinct tasks in the metabolism, which makes accurate identification crucial. In recent years awareness has grown that lipid analysis must provide complete structural elucidation of individual species including isomers.[2–3] Only then can their biological functions, distribution in tissue and involvement in metabolic pathways be comprehensively understood.

Mass spectrometry (MS) is unquestionably the dominating technology in lipidomics.[4] In the past years, lipid analysis has greatly benefited from the emergence of novel separation, derivatization, ion activation and imaging techniques.[2–3,4b,5] A series of promising approaches use laser light in the ultraviolet (UV) or infrared (IR) range to dissociate molecular ions at a fixed photon energy[6] or to perform action ion spectroscopy[7] using tunable light sources. These techniques are increasingly being applied to lipids and deserve particular attention because of their high diagnostic potential and progressing commercialization of the respective instrumentation. Photofragmentation of molecular ions yields complementary information to more established ion activation techniques in tandem MS (MS/MS) by offering alternative fragmentation mechanisms.[6a–d] Furthermore, by extending the excitation wavelength from a fixed value to a continuous range, molecular fingerprints in the IR and UV region can be obtained.[7] Spectroscopy of ions is predestined for the identification of metabolites and distinction of isomers because of its sensitivity towards subtle structural modifications.[7h,8]

Here we provide an overview on the emerging field of lipid analysis using UV and IR laser light in combination with MS. First, we outline the merits of UV photodissociation (UVPD) and IR multiple photon dissociation (IRMPD) for lipid fragmentation at a fixed wavelength. We then focus on the development of derivatization methods to increase the absorption coefficient of intrinsically UV-inactive lipids and to induce alternative fragmentation pathways. In the second part, we explain the extension of single-wavelength photofragmentation to UV and IR action ion spectroscopy and present several experimental approaches and applications for lipid analysis. Finally, we provide an outlook on instrumental developments and future applications. Throughout this review, lipid analysis is in the spot light; however, a few studies on other metabolites from which lipid analysis is expected to benefit are discussed as well. In order to set the frame for lipid classification and nomenclature employed throughout the review, the LIPID MAPS classification system for lipids is introduced in the following section.

1.1. Lipid classification and annotation

Historically, lipids have been broadly defined by their hydrophobicity and solubility in non-polar solvents.[9] In an effort to support the emerging field of lipidomics in the early 2000s, the International Lipid Classification and Nomenclature Committee established a clear definition along with a comprehensive classification system for lipids.[10] Henceforth, lipids were specified as *hydrophobic or amphipathic small molecules that may originate entirely or in part by carbanion-based condensations of thioesters and/or by carbocation-based condensations of isoprene units.*[10] The LIPID MAPS classification system organizes lipids into eight categories based on their chemical structures: fatty acyls (FA), glycerolipids (GL), glycerophospholipids (GP), sphingolipids (SP), saccharolipids (SL), polyketides (PK), prenol lipids (PR), and sterol lipids (ST) (Figure 1A). Each category is further ramified into classes and subclasses, which form the framework of the LIPID MAPS Structure Database.[11] Along with the classification system, recommendations for lipid nomenclature and structure drawing were released, which are continuously being updated and extended.[12]

[a] C. Kirschbaum, K. Pagel
Institut für Chemie und Biochemie
Freie Universität Berlin
Altensteinstraße 23a
14195 Berlin (Germany)
[b] C. Kirschbaum, K. Pagel
Fritz-Haber-Institut der Max-Planck-Gesellschaft
Faradayweg 4–6
14195 Berlin (Germany)
E-mail: ckirschbaum@fhi-berlin.mpg.de

Review
doi.org/10.1002/anse.202200103
Chemistry Europe
European Chemical Societies Publishing

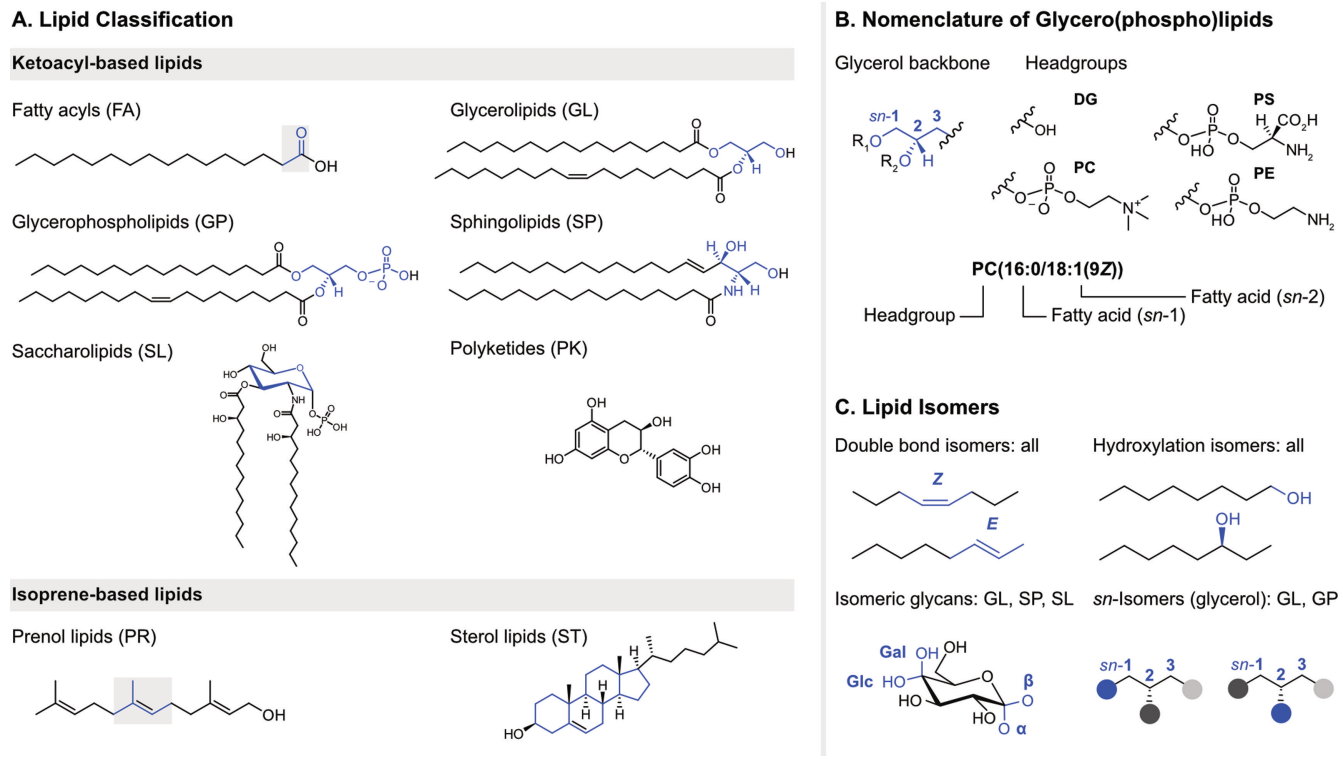

Figure 1. (A) Classification of lipids into eight categories. A representative example for each category is shown with the common structural motif highlighted in blue. Prenol- and sterol lipids are for the most part derived from condensation of isoprene, whereas lipids from the remaining categories are synthesized by the condensation of thioesters. (B) Nomenclature of glycerolipids and glycerophospholipids. The lipid class is defined by the headgroup, yielding, for example, diacylglycerols (DG), phosphatidylcholines (PC), phosphatidylserines (PS) or phosphatidylethanolamines (PE). The shorthand notation for 1-palmitoyl-2-oleoyl-*sn*-glycero-3-phosphocholine is exemplarily shown. (C) Examples of lipid isomers that are challenging to distinguish by mass spectrometry. Some isomers are typical for specific lipid categories. Glc = glucose; Gal = galactose.

Based on the LIPID MAPS terminology, a shorthand nomenclature for lipids was developed to promote the unified reporting of MS data and facilitate inter-laboratory comparison.[13] The shorthand notation encodes which structural details were resolved by MS and which remained undetermined. For example, glycerolipids can be analyzed on different levels of complexity (Figure 1B).[13e] The lowest, *lipid class level* is determined by the molecular weight and the headgroup attached to the *sn*-3 position of the glycerol backbone. Glycerophospholipid classes are, for example, phosphatidylcholine (PC), phosphatidylethanolamine (PE) or phosphatidylserine (PS). The second level of complexity is the *bond type level*, which defines the bond type (ester, alkyl-, or alk-1-enyl-ether) by which lipid chains are linked to the glycerol backbone. On the *fatty acyl level*, the fatty acyl identities, *i.e.*, their length and number of unsaturations are determined. In the shorthand nomenclature for fatty acyls, the number of carbon atoms is separated by a colon from the number of double bonds. The *fatty acyl position level* determines the *sn*-positions of the lipid chains on the glycerol backbone. If the regiochemistry is undefined, the two fatty acyls are separated by an underscore; otherwise by a forward slash with *sn*-1 placed before and *sn*-2 behind the slash. On the highest level of complexity, the location and configuration of carbon-carbon double bonds are specified in brackets. The double bond position is counted starting from the carbonyl carbon of the fatty acid, and its configuration is given as *Z* (*cis*), *E* (*trans*) or Δ (unknown).

A lipid defined at the *lipid class level* might contain dozens of isomeric structures (Figure 1C).[2] In addition to double

Carla Kirschbaum is a PhD student at Freie Universität Berlin and guest scientist at the Fritz Haber Institute of the Max Planck Society. Her research is focused on lipid analysis using innovative mass spectrometry-based techniques such as ion mobility-mass spectrometry and gas-phase infrared spectroscopy.

Kevin Pagel is a professor at Freie Universität Berlin and guest researcher at the Fritz Haber Institute of the Max Planck Society. The central topic of his research is the structural analysis of biological macromolecules and their complexes using gas-phase techniques, in particular glycans, glycoconjugates and lipids.

bonds, other chain modifications such as hydroxylation give rise to regio- and stereoisomers. Furthermore, in glycerol-based lipids, fatty acyls can be attached at three different positions of the glycerol backbone, yielding *sn*-isomers. In saccharolipids and glycolipids, the structural diversity of lipids is potentiated by the immense complexity of sugar structures.[14] Isomeric sugars often differ in a single stereocenter, such as glucose (Glc) and galactose (Gal) or α- and β-sugars. When reporting MS data, the annotation should clearly convey which isomers were resolved to avoid erroneous biological interpretations.[13b] The shorthand nomenclature was recently updated[12b] and integrated into the latest version of a grammar-based computational library for lipid names.[15] Furthermore, a freely available checklist was recently developed to support the standardized reporting of lipidomics data.[16]

2. Photodissociation of lipids in tandem mass spectrometry

2.1. Photodissociation schemes

The past years have witnessed a surge in novel ion activation techniques to extract a maximum of structural information from MS/MS experiments.[2–3,4b,5b–d] Molecular ions can be fragmented by collision-, electron- and photon-based approaches, which deposit sufficient internal energy to overcome the dissociation threshold. Collision-induced dissociation (CID) is the most widespread ion activation technique but usually insufficient for complete structural characterization of lipids.[4a] Complementary structural information can be obtained by photodissociation techniques that induce alternative fragmentation pathways in dependence of the photon energy. UVPD employs UV photons to excite molecular ions from the ground electronic state S_0 into an excited electronic state S_1 (Figure 2).[6c] Subsequently, dissociation can occur directly from the excited state S_1 (1), by relaxation into a dissociative state (2), or from the vibrationally excited ground electronic state S_0 following internal conversion (3).[7d,17] These processes usually occur between femtoseconds and several hundred picoseconds.[17] The energy of a single 200 nm UV photon is about 6 eV (600 kJ mol^{-1}) and thus sufficient for the fragmentation of typical chemical bonds in organic molecules (300–500 kJ mol^{-1}).

On the contrary, the energy of an IR photon (10.6 μm) is in the range of 0.1 eV (10 kJ mol^{-1}). Because the energy acquired by photoexcitation must exceed the dissociation threshold of the electronic ground state, dozens to hundreds of IR photons must be sequentially absorbed by the ion in a process called infrared multiple photon dissociation (IRMPD).[6d,7b] After the absorption of each photon, the energy is dispersed within the molecular ion by intramolecular vibrational redistribution, which allows for the incremental increase of the internal energy until the weakest bonds break.[19] IRMPD is classified as a slow heating method like CID, and both methods often yield similar fragments.[18] UVPD, on the contrary, is a fast dissociation

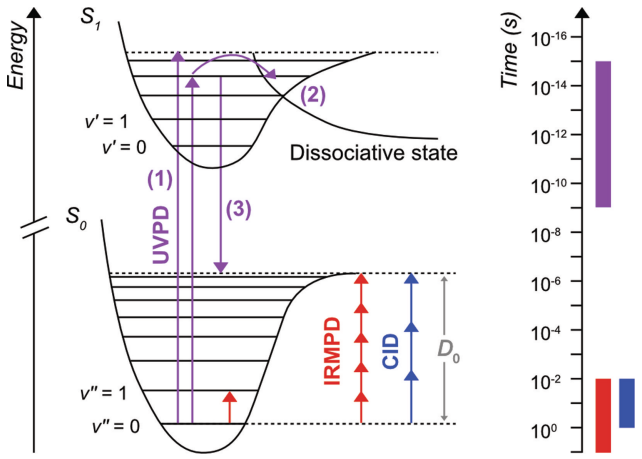

Figure 2. Schematic energy and time diagrams illustrating the ultraviolet photodissociation and infrared multiple photon dissociation processes in comparison with classical collision-induced dissociation. Closed-shell ions are excited from the ground electronic state S_0 to an excited electronic state S_1 by a UV photon, which can lead to direct dissociation (1), relaxation into a dissociative state (2), or dissociation from the ground electronic state following internal conversion (3). IR photons induce vibrational excitation in the ground electronic state until the dissociation threshold D_0 is reached. The timings adapted from [18] divide the techniques into fast (UVPD) and slow (IRMPD and CID) ion activation methods.

method, which usually yields more complex fragmentation patterns due to the high photon energy and multitude of UV-triggered photochemical processes. In polyanions, UV absorption can lead to electron photodetachment (EPD). EPD yields charge-reduced radical anions, which can be dissociated by collisions in a process called activated electron photodetachment (a-EPD).[20]

2.2. Infrared multiple photon dissociation

IRMPD of molecular ions induces photofragmentation by the sequential absorption of multiple IR photons. The technique was first implemented in Fourier-transform ion cyclotron resonance (FTICR) mass spectrometers and proved its applicability for the structural analysis of biomolecules.[21] Subsequently, IRMPD was also integrated into commercial quadrupole ion traps.[6d] The most popular light source for IRMPD are CO_2 lasers, which provide IR radiation centered around 10.6 μm. IRMPD does oftentimes not provide additional information on lipid structures compared with conventional CID.[4b] However, a major advantage of IRMPD photodissociation is that the laser wavelength offers a certain degree of selectivity. Lipids and metabolites containing phosphate and sulfate groups were found to be more efficiently fragmented by 10.6 μm photons than non-phosphorylated or -sulfated analogs.[4b] Consequently, IRMPD yields complementary structural information to CID for nucleotides and phosphorylated sugars, particularly with increasing number of phosphates.[22] Transferred to lipid analysis, these findings imply that phosphorylated lipids including phosphatidylinositols, lipid A and larger lipopolysaccharides are suitable candidates for IRMPD.

Lipid A is the saccharolipid core structure and membrane anchor of lipopolysaccharides, which constitute the outer membrane of Gram-negative bacteria.[1] The lipid A core consists of a conserved diglucosamine disaccharide modified with largely varying fatty acids, phosphates and additional monosaccharides (Figure 3A). The virulence of lipopolysaccharides depends strongly on structural modifications including the phosphorylation pattern on the lipid A core.[23] Because the photoabsorption cross section in IRMPD increases with increasing degree of phosphorylation, product ions of lipid A with different number of phosphate groups can be readily differentiated.[24] The efficient fragmentation of phosphate-containing fragments manifests itself in the absence of bisphosphorylated ions in the photodissociation spectra and emergence of secondary photofragment ions in the lower mass range (Figure 3B). The increased abundance of fragments and determination of the phosphorylation status by IRMPD facilitate structural assignment. Furthermore, IRMPD was used to demonstrate that some Gram-negative bacteria produce pyrophosphorylated lipid A in addition to the more common bisphosphorylated species carrying two monophosphates.[25] Also more complex lipopolysaccharides isolated from bacteria were investigated by IRMPD in negative ion mode.[26] The absorption of 10.6 μm IR photons induced glycosidic bond cleavage between the conservative inner and variable outer core oligosaccharide regions. In combination with other fragmentation techniques, IRMPD helped to confirm known and discover new core oligosaccharide structures in bacterial lipopolysaccharides.[26a]

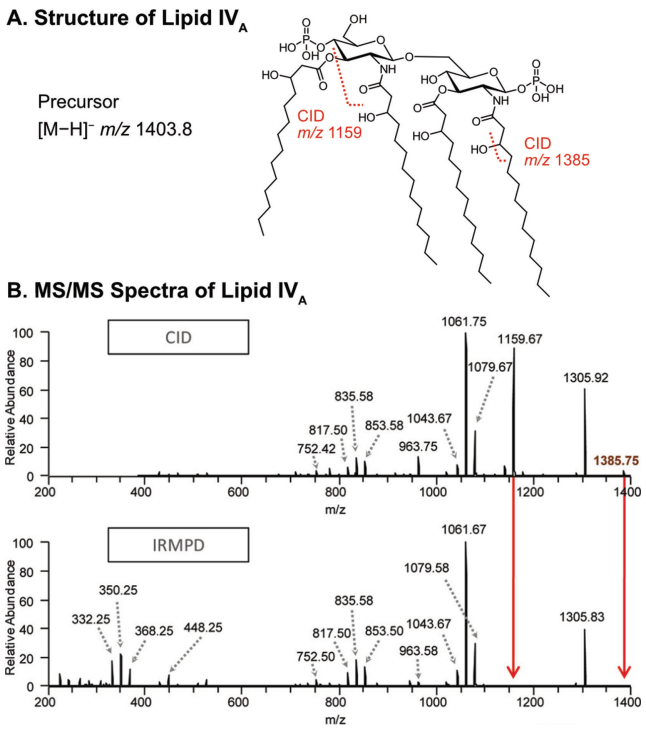

Figure 3. Dissociation of deprotonated lipid IV$_A$. (A) Structure of lipid IV$_A$ and formation of bisphosphorylated fragment ions by collision-induced dissociation. (B) Comparison between collision-induced dissociation and infrared multiple photon dissociation of deprotonated lipid IV$_A$. Two bisphosphorylated product ions (*m/z* 1159.67 and 1385.75) are absent in the IRMPD spectrum because they are efficiently fragmented. Additional fragment ions below *m/z* 500 arise from secondary photofragmentation. Adapted with permission from [24]. Copyright 2011 American Chemical Society.

Another type of lipids that were studied by IRMPD are phosphatidylinositols, a class of glycerophospholipids with signalling activities.[1] Phosphatidylinositols carry an inositol headgroup, which is often phosphorylated. MS/MS fragmentation of phosphatidylinositols with varying degrees of phosphorylation was studied by IRMPD.[27] In accordance with previous CID experiments,[28] the fatty acids were identified and the number of phosphates but not their positions determined. Furthermore, evidence for phosphate migration from the inositol headgroup to the glycerol backbone was provided. In a different study, bacterial phosphatidylinositol mannosides were investigated by IRMPD in negative ion mode to determine the structure of fatty acids at different acylation sites.[29] In combination with positive ion mode CID, the fatty acids at four possible acylation sites on the glycerol backbone, inositol and mannose were located.

A few non-phosphorylated lipids were investigated by IRMPD as well. For instance, the ganglioside GM1 was investigated by several FTICR ion activation techniques including IRMPD.[30] IRMPD was outperformed by electron capture dissociation (ECD), which yielded more structural information about the glycosphingolipid with less experimental adjustments necessary. However, IRMPD has the advantage that the degree of fragmentation can be controlled by the duration of laser irradiation and yields information on relative bond stabilities. In a different FTICR MS/MS experiment, the performances of IRMPD and CID for the structural identification of hydroxylated eicosanoids were compared.[31] Eicosanoids are metabolites of arachidonic acid and play important roles as lipid mediators, *e.g.* in inflammation.[1] The IRMPD fragmentation patterns reflect the number and position of hydroxyl groups, which enabled the identification of regioisomers in trihydroxylated eicosanoids. Overall, studies on lipids using fixed-wavelength IRMPD are rare because the gain in structural information compared to CID is limited to specific, mostly phosphorylated, lipid classes. As will be shown in Section 4, the extension of IRMPD to a continuous wavelength range significantly increases the gain in structural information and renders the technique more generally applicable.

Beyond the investigation of isolated lipid ions, IRMPD has been harnessed to study membrane protein-bound lipids.[32] Membrane protein assemblies are usually extracted from cell membranes and brought into the gas phase using detergents.[33] Subsequently, the detergent micelle must be removed by gas-phase activation techniques, such as CID or IRMPD. IRMPD activation offers several advantages over CID because fragmentation is charge-state independent and can be increased by increasing the energy of the external laser without compromising the ion transfer in the mass spectrometer. It was shown that IRMPD is sufficiently gentle to liberate intact, non-covalent membrane protein-lipid complexes from detergent micelles (Figure 4A). Furthermore, combining CID and IRMPD allowed to first release the complexes from micelles by colli-

Review
doi.org/10.1002/anse.202200103

Chemistry Europe
European Chemical Societies Publishing

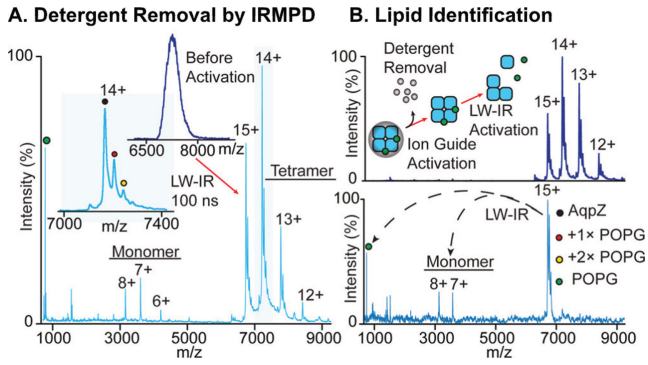

Figure 4. Detergent removal and release of lipids from membrane protein complexes. (A) Intact membrane proteins (here Aquaporin-Z tetramer) with specifically bound lipids can be liberated from micelles by infrared multiple photon dissociation. (B) Sequential CID (top), mass selection, and IRMPD (bottom) enable the identification of the protein stoichiometry and mass of protein-bound lipids in a single experiment. AqpZ = Aquaporin-Z; POPG = 1-palmitoyl-2-oleoyl-*sn*-glycero-3-phosphoglycerol. Reprinted with permission from [32]. Copyright 2016 American Chemical Society.

sional activation, isolate the detergent-free complex, and then dissociate the complex by IRMPD (Figure 4B). Thus, the protein subunit stoichiometry and the lipid mass were determined in a single experiment. The approach is highly valuable to identify lipids that specifically bind to membrane proteins and modulate their functions. One particularly interesting family of membrane proteins in this regard are G-protein-coupled receptors (GPCRs). They trigger intracellular signalling cascades and represent the most intensively studied drug targets: one third of the currently approved drugs act on GPCRs.[34] Because the structure and function of GPCRs are influenced by the surrounding membrane lipids, understanding the interplay between lipid composition and receptor functioning could help to develop new therapeutical approaches.[35]

2.3. Ultraviolet photodissociation

In UVPD, ions are dissociated by the absorption of high-energy photons. Consequently, extensive fragmentation is induced via dissociation pathways that are inaccessible by low-energy CID and IRMPD. UVPD was first implemented in an FTICR mass spectrometer[36] and has since been mainly but not exclusively used in combination with ion trap mass spectrometers.[6c] The first commercial Orbitrap mass spectrometer equipped with a solid-state laser (213 nm) for UVPD was recently introduced.[37] Higher photon energies are provided by F_2 (157 nm) and ArF (193 nm) excimer lasers, which require familiarity with laser set-up and some customization of the mass spectrometer hardware and/or software. Usually, the lasers are pulsed to deliver a high photon flux on short timescales.[6c]

193 nm UVPD has been employed to identify key structural features in a variety of different lipid classes including glycerophospholipids, glycosphingolipids, lipid A and larger lipopolysaccharides.[6b,c] In glycerolipid analysis, the technique filled two major gaps at once: pinpointing double bonds and determining the *sn*-position of fatty acids on the glycerol backbone. UVPD was initially found to yield pairs of product ions separated by 24 Da for unsaturated PC ions, which derive from cleavage of the C–C bonds adjacent to the double bond.[38] The diagnostic pairs of fragments allow to determine the positions of C=C bonds and to distinguish PC double bond isomers. The technique was integrated into a liquid chromatography (LC)–MS workflow using parallel reaction monitoring for complementary separation and identification of PC double bond isomers.[39] The workflow allowed for relative quantification of double bond isomers by probing double bond diagnostic precursor-to-fragment ion transitions. The signal-to-noise ratio (*s/n*) of diagnostic fragments revealing the double bond position in glycerophospholipids can be significantly enhanced by the elimination of undissociated precursor ions.[40] Hybrid higher-energy collisional dissociation (HCD)/UVPD fragmentation of PC ions was demonstrated to determine not only double bond positions within the lipid chains but also *sn*-positions of the fatty acyls on the glycerol backbone.[41] In the first step, HCD of sodiated PC generates dioxolane fragments, which are then dissociated by UVPD via cross-ring and allylic cleavage into *sn*- and double bond-specific fragments (Figure 5). The hybrid HCD/UVPD workflow thus provides near-complete structure elucidation of glycerophospholipids.

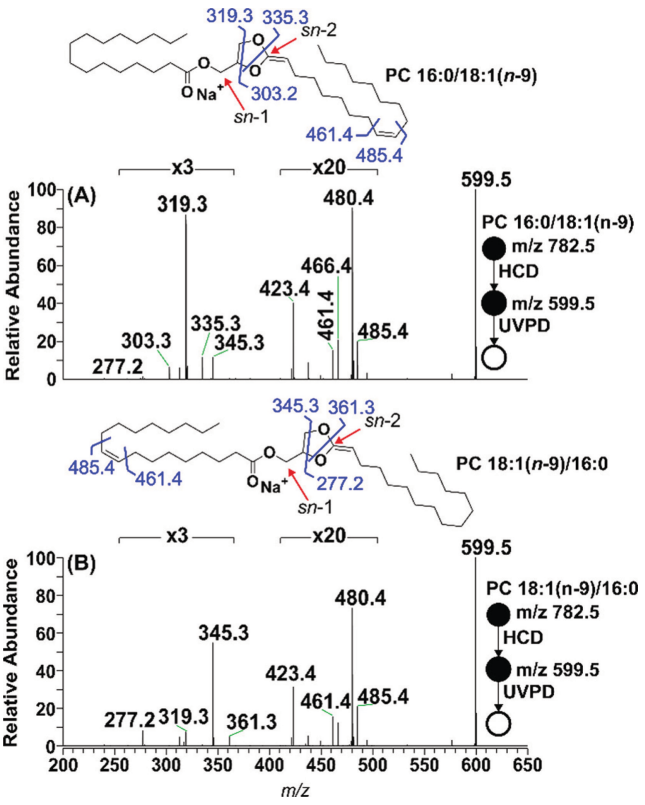

Figure 5. Tandem mass spectrometry employing hybrid collision-based dissociation followed by ultraviolet photodissociation yields *sn*- and double bond positions in glycerophospholipids. Higher-energy collisional dissociation generates a five-membered dioxolane ring, which yields double bond- and *sn*-diagnostic fragments upon irradiation with 193 nm UV photons. Reprinted with permission from [41]. Copyright 2017 American Chemical Society.

In combination with desorption electrospray ionization (DESI), UVPD can identify the spatial distribution of PC double bond isomers in tissues.[42] Differences in the distribution of individual isomers that remain unresolved in DESI-MS were identified in different tissue regions, particularly between healthy and cancerous tissue. The technique was slightly modified to investigate double bond isomers of free fatty acids in biological samples with reactive DESI.[43] Charge-inverted dication-fatty acid complexes were generated *in situ* on the tissue and subjected to UVPD in positive ion mode. Even though the sensitivity was not sufficient to identify low-abundant polyunsaturated fatty acids, it was possible to determine the $9\Delta:11\Delta$ double bond ratio of 18:1 fatty acids in different breast cancer subtypes. The general utility of 193 nm UVPD for structure elucidation of unsaturated fatty acids was assessed in a systematic study taking into account monounsaturated and conjugated or non-conjugated polyunsaturated fatty acids with different number and positions of unsaturations.[44] The comprehensive results demonstrate that UVPD provides detailed structural characterization of lithiated unsaturated fatty acids and even enables the relative quantification of isomeric mixtures.

For glycerophospholipid classes that preferentially ionize with negative polarity, the same double bond diagnostic fragment ions spaced by 24 Da as in positive ion mode were observed.[45] LC-UVPD in negative ion mode revealed species-specific distributions of isomers in bacterial glycerophospholipids.[45] In a more comprehensive study on the wealth of bacterial glycerophospholipid modifications, acyl chain and headgroup modifications were identified that are not listed in MS/MS databases and call for further investigation.[46] The results obtained for glycerophospholipids were extended to cardiolipins, which are found in bacterial and mitochondrial membranes.[47] They consist of two phosphatidic acids connected at the phosphates via a central glycerol and carry four instead of two fatty acyls.[1] Hybrid CID/UVPD in negative ion mode enabled to locate double bonds and cyclopropane modifications in all fatty acids.[47a] Cyclopropane modifications are frequent in bacterial lipids and related to enhanced stress responses.[1] Similar to the localization of double bonds, UVPD of cyclopropane fatty acids generates diagnostic pairs of ions separated by 14 Da in both ion modes, which arise from cross-ring cleavage on both sides of the ring. Fragments diagnostic for *sn*-positions, however, could only be generated in positive ion mode. Therefore, an improved procedure for cardiolipin analysis was developed, which relies on methylation of the phosphates to increase the ionization efficiency in positive polarity.[47b] Hybrid HCD/UVPD of metal-cationized methylated cardiolipins afforded both double bond and *sn*-position specific fragmentation. The procedure is expected to be transferable to other anionic glycerophospholipids as well.

Glycosylated lipids including mainly lipooligosaccharides and their core structure lipid A,[24,48] but also glycosphingolipids[49] were analyzed by UVPD at 193 nm. The structure of lipid A accounts for an important part of the toxicity of lipopolysaccharides and is therefore often studied after mild-acid hydrolysis.[50] In an initial study, UVPD of lipid A was found to yield a range of fragments that are not accessible by CID and IRMPD.[24] Cross-ring and glycosidic cleavage between the central glucosamine units yield information about the connectivity of acyl chains. Furthermore, cleavage of C–C bonds next to carbonyl or hydroxyl groups as well as cleavage of C–O and amide bonds facilitate the identification of acyl chains. a-EPD of bisphosphorylated lipid A anions yielded similar fragmentation patterns as UVPD with enhanced cross-ring fragmentation and preferential cleavage next to carbonyl bonds. Following this initial investigation, UVPD was applied in a number of studies to identify unique structural modifications of lipid A in different bacteria.[48a–f] Higher-throughput analysis of complex lipid A mixtures was achieved by integrating UVPD into an LC–MS workflow.[48g] Because UVPD of lipid A yields complex fragmentation patterns that are difficult to interpret, an automated approach for data acquisition and interpretation was developed.[48h] It allows to identify acyl chain length and linkage in bisphosphorylated lipid A by employing two-step activation. Doubly charged anions are subjected to UVPD and CID without intermediate mass isolation. Hence, both UVPD and a-EPD fragments are generated, which provide rich structural information in one activation step. The approach does not rely on databases and is thus suitable for *de novo* identification of lipid A structures. A different approach employs the reversed CID/UVPD MS^3 activation scheme to map phosphate modifications in lipid A.[48i] In the first step, substituted lipid A is subjected to CID to identify key acyl chain losses and concurrently get rid of isobaric non-lipid A species. In the second stage, UVPD is applied to the acyl chain loss product ion to identify and localize phosphate substitutions. With the aim to refine automated workflows by establishing predictive rules for lipid A fragmentation, fragmentation pathways were monitored by energy-resolved CID, HCD and UVPD.[48j] The most comprehensive information on sequential fragmentation pathways were obtained by HCD, which allowed to establish rules for the preferential cleavage of acyl chains. UVPD yielded less differentiated information because of the high internal energy deposition.

In bacterial lipooligosaccharides, the lipid A anchor is equipped with core polysaccharides, which are further elongated by an *O*-antigen polysaccharide tail in lipopolysaccharides.[48k] With increasing molecular complexity, hybrid MS/MS techniques become indispensable for reliable structural analysis. For lipooligosaccharide profiling, an LC–MS/MS workflow combining UVPD and HCD was developed, which was shown to provide a greater dissociation efficiency than UVPD alone.[48k] In addition to collision-induced glycosidic bond cleavage, UVPD yields abundant C–C, C–O, C–N and cross-ring cleavages, which provide crucial information on the lipid A core and polysaccharide branching. An alternative approach employs hybrid CID/UVPD for shotgun analysis, *i.e.*, without chromatographic separation.[48l] CID induces cleavage of the weak glycosidic bond between lipid A and the core oligosaccharides, which both yield abundant product ions. Following isolation, UVPD applied to each portion of the molecule reveals a wealth of information such as saccharide connectivity by cross-ring cleavage. To reduce the inherent spectral complexity

of shotgun mass spectra, the workflow was extended by an LC separation protocol for lipooligosaccharides.[48m] Following the separation, intact lipooligosaccharides from antibiotic-resistant bacteria were analyzed by CID/UVPD and CID/HCD. Ion mobility spectrometry (IMS) has been employed as well to separate lipooligosaccharides from isobars and characterize a chemically modified lipooligosaccharide vaccine candidate.[48n] Current bottlenecks in lipooligosaccharide analysis are the tedious extraction from bacteria and complex, non-automated data analysis.[48m,n]

Glycosphingolipids pose similar analytical challenges as lipid A and lipooligosaccharides. They consist of a hydrophilic glycan, which is glycosidically linked to a hydrophobic ceramide consisting of a sphingolipid and an amide-linked fatty acid.[1] Contrary to lipid A, no additional lipid chains are attached to the sugar backbone.[10] 193 nm UVPD was employed to study neutral and acidic glycosphingolipids.[49] Whereas collision-based methods mainly induced glycosidic bond cleavage, UVPD yielded cross-ring and lipid-related fragments. Thus, UVPD afforded differentiation between isomeric glycans and ceramides. The general utility of UVPD in sphingolipid analysis was demonstrated in a comprehensive study including a range of different sphingolipids and glycosphingolipids.[51] In particular, cleavage of C–C bonds next to unsaturations reliably locates double bonds in sphingosine and fatty acids in positive ion mode. Additional fragments specify the identity of the headgroup and both lipid chains. Overall, 193 nm UVPD is a powerful technique for top-down lipid analysis and has the potential to be integrated into high-throughput workflows.

With the introduction of the first commercial Orbitrap mass spectrometer featuring UVPD, the technique became applicable to non-specialized laboratories.[6c] However, the instrument is equipped with a 213 nm solid-state laser providing lower photon energy (5.8 eV per photon) than 193 nm ArF excimer lasers (6.4 eV per photon). To assess the performance of 213 nm vs. 193 nm UVPD, bacterial glycerophospholipids and mycolic acid were investigated at both wavelengths to identify cyclopropane modifications.[37] Diagnostic pairs of fragment ions spaced by 14 Da were generated at both wavelengths; however, at lower abundance and with longer activation periods (200 ms vs. 20 ms) required for 213 nm irradiation. Nonetheless, the 213 nm option provides a viable alternative, which was capable of analyzing complex bacterial lipid extracts in LC–MS. LC–MS coupled with 213 nm irradiation was further employed to distinguish between plasmenyl (vinyl ether linkage) and plasmanyl (ether linkage) glycerophospholipids with simultaneous localization of C=C bonds in the lipid chains.[52] The investigated ether- and vinyl ether-linked glycerophospholipids are often isomeric and difficult to differentiate by conventional techniques. In a different study, 213 nm UVPD was harnessed for complete structural elucidation of fatty acid esters of hydroxy fatty acids.[53] These recently discovered, bioactive lipids exert anti-diabetic and anti-inflammatory functions.[54] CID and HCD allow to determine the identities of the esterified fatty acid and the hydroxy fatty acid but provide no information about the position of esterification. On the contrary, hybrid HCD/UVPD is able to pinpoint the position of the ester bond and furthermore the positions of unsaturations within the two lipid chains in lithiated analytes. HCD of the precursor ions dissociates the ester and leaves behind the individual fatty acids with a double bond on either side of the original ester bond, which can be readily identified by UVPD. Because the technique does not rely on reference spectra, it has the potential to be employed for *de novo* identification of fatty esters. In a different study, cationic sterol lipids irradiated at 213 nm were found to yield $[M]^{+\cdot}$ radical cations. Subsequent HCD dissociates them into informative fragments similar to those observed upon electron ionization.[55] Hence, using soft electrospray ionization (ESI) and hybrid 213 nm photodissociation multistage tandem MS, structural information was obtained that afforded distinction between isomeric oxysterols.

To better understand the mechanism of UVPD in the absence of gas collisions, the impact of the laser fluence and the number of laser pulses on the photofragmentation was studied in a custom-built two-wavelength (213 nm and 266 nm) UVPD setup coupled to an FTICR mass spectrometer.[56] Cationization of PC(18:1(9*Z*)/18:1(9*Z*)) with UV-absorbing Fe^{2+} significantly boosted the photofragmentation yield and enabled dose and fluence dependent measurements. The results suggest that Fe^{2+}-cationized PC dissociates in a single-photon process at 213 nm. Fe^{2+} complexation and 213 nm UV radiation were used for relative quantification of PC *sn*-isomers based on the preferential formation of *sn*-2 associated product ions.[57] However, the approach is less universally applicable to glycerophospholipids than the hybrid HCD/UVPD (193 nm) approach discussed above[41] because Fe^{2+} adduction was only observed for PC. Lipids were also investigated at very high photon energies (7.9 eV per photon) provided by a 157 nm F_2 excimer laser.[58] UVPD of two isomeric leukotrienes yielded informative radical fragment ions that are not observed in CID or HCD and allowed for isomer differentiation.

For the analysis of complex mixtures, separation techniques such as LC are usually required. Alternatively, UVPD has been coupled with IMS.[59] In this gas-phase electrophoretic separation technique, ions traverse a buffer gas-filled cell under the influence of an electric field.[60] They are separated based on differences in their gas-phase mobility, which is determined by their mass, charge, size and shape. The collision cross section (CCS) can be determined as an instrument-independent parameter. UVPD was first implemented in custom-built drift tube (DT) ion mobility mass spectrometers in combination with ion traps[59a] and time-of-flight (TOF) MS.[59b] Tandem ion mobility enabling mobility selection of precursor ions and mobility measurement of photofragmentation products was achieved by a dual drift tube system separated by a laser interaction region.[59c] After the commercialization of ion mobility mass spectrometers, a TOF mass spectrometer equipped with travelling wave (TW) ion mobility was modified to enable UVPD.[59d] Eventually, DTIMS was coupled with a hybrid ion trap/Orbitrap mass spectrometer modified with a 193 nm UV laser and used to analyze PC double bond isomers.[59e] Even though the resolving power of DTIMS is usually insufficient to separate phospholipid isomers,[61] the

drift time profiles of isomers could be extracted by applying UVPD after the ion mobility separation, which yields isomer-specific fragments. Thus, double bond or cyclopropane positions and accurate CCS of PC isomers were determined, even though the isomers were only partially resolved in the mobility dimension (Figure 6). The use of absorption mode Fourier transform multiplexing significantly increased the resolution and *s/n* of drift time profiles. In principle, the technique is applicable to all kinds of lipid isomers that produce unique fragments upon UVPD.

2.4. Derivatization strategies

One major impediment to the application of UVPD for lipid analysis is that the fragmentation efficiency is determined by the absorbance of functional groups. Most lipids do not contain UV chromophores and only start absorbing UV light below 220 nm.[56] Consequently, tailor-made UV chromophores have been attached to lipids to increase the overall UV absorbance, shift the absorption wavelength into the range of commercial solid-state UV lasers, and induce specific dissociation mechanisms. One such approach that has been adopted from proteomics is radical-directed dissociation (RDD).[62] In this technique, the analyte is covalently or non-covalently modified by a photocaged radical precursor that forms a radical upon UV irradiation inside the mass spectrometer. Following the photoactivation, CID induces radical driven fragmentation similar to a-EPD. Radicals can also be directly formed by CID without the need for photoactivation, which is, however, less common.[63] Radical precursors for lipid analysis are bifunctional molecules: in addition to the radical initiator, they contain a variable region for lipid attachment.[64] In the first study applying RDD for lipid analysis, non-covalent complexes of glycerophospholipids, sphingolipids and triacylglycerols with 4-iodoaniline and 4-iodobenzoic acid were formed by ESI.[64a] Irradiation with 266 nm UV light caused homolytic cleavage of the weak C–I bond, generating substituted phenyl radicals. Collision-induced

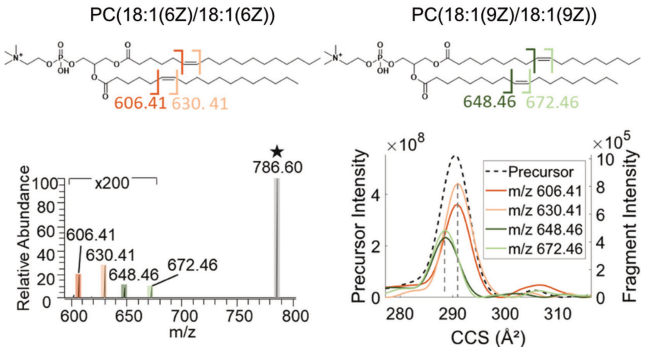

Figure 6. Coupling of drift tube ion mobility spectrometry with ultraviolet photodissociation mass spectrometry. UVPD of the isomeric phosphatidylcholines PC(18:1(6*Z*)/18:1(6*Z*)) and PC(18:1(9*Z*)/18:1(9*Z*)) at *m/z* 786 (1+) yields double bond-specific pairs of fragments. Drift time profiles of the isomers are extracted from the arrival time distribution of the mixture using Fourier transform multiplexing. Reprinted with permission from [59e]. Copyright 2022 American Chemical Society.

RDD of the radical cations or anions induced intrachain fragmentation revealing the location of double bonds and chain branching.[64a] For smaller fatty acids, non-covalent modification with 4-iodoaniline did not yield radical cations incorporating the lipid.[64b] Instead, covalent derivatization of fatty acids as 4-iodobenzoic esters was applied to determine the position of double bonds, chain branching and hydroxylation. The double bond geometry remained undetermined in that study. On the contrary, CID of proton-bound complexes of fatty acid methyl esters with 4-iodoaniline rendered *Z* and *E* double bonds as well as conjugated and non-conjugated double bonds distinguishable; however, only in the absence of UV irradiation.[65] Moreover, by employing diiodoanlines instead of iodoanilines, lipids can be cross-linked by the generation of aniline biradicals upon 266 nm irradiation.[66] The cross-linking efficiency of triacylglycerols was found to depend on the number of double bonds in the fatty acid chains.

In general, the fragmentation pathways induced by a specific radical initiator are impossible to predict. Therefore, systematic empirical studies are required to determine the derivative which fits the specific lipid class and research question best. For fatty acid analysis, fixed-charge pyridinium derivatives were developed to increase the ionization efficiency in positive ion mode and simultaneously enable photodissociation at 266 nm.[67] The radical initiator is covalently attached to the fatty acids via an amide linker (Figure 7A). One of the developed pyridinium derivatives, 1-(3-(aminomethyl)-4-iodophenyl)pyridin-1-ium (4-I-AMPP$^+$), was employed to study unsaturated, branched and hydroxy fatty acids.[67–68] Isomeric fatty acids differing in the position of unsaturation, methyl branching or cyclopropanation were identified by diagnostic fragments (Figure 7B).[67] Irradiation of 4-I-AMPP$^+$-modified (*O*-acyl)-ω-hydroxy fatty acids at 266 nm followed by CID induced intra-chain carbon-carbon cleavage without interruption, which confirmed a straight-chain structure.[68a] RDD of hydroxylated fatty acids yielded fragments that indicated locations of double bonds and hydroxyl groups.[68b] By integrating the photodissociation technique into an LC–MS workflow, modified isomeric eicosanoids were separated and identified. Further refinement of the molecular structure yielded the next-generation radical initiator *N*-(2-aminoethyl)-4-iodobenzamide, which boosted the photoproduct yield from $<30\,\%$ to $>95\,\%$ by shifting the absorption maximum of derivatized fatty acids exactly into the 266 nm region.[69]

By tailoring the lipid-adducting portion of the derivatization agents, individual lipid classes can be selectively modified. Crown ethers are known to form complexes with protonated primary amines present in phosphatidylethanolamines (PE)[70] and other glycerophospholipids[71] as well as lyso-glycosphingolipids.[72] In PE analysis, iodobenzoyl-modified crown ethers fulfil a dual purpose: they efficiently differentiate PE from isomeric PC and shift PE to significantly higher masses by non-covalent adduct formation. Secondly, the iodobenzoyl moiety enables RDD of the PE-crown ether complexes, which reveals double bond location and chain branching. The technique was transferred to a range of amine-containing glycerophospholipids including phosphatidylserine (PS), and

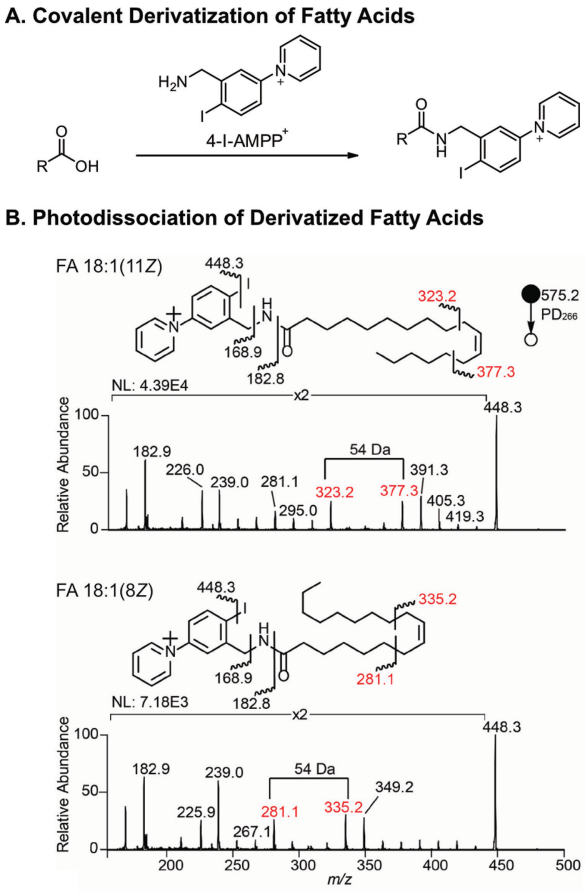

Figure 7. Covalent modification of fatty acids by radical precursors enables the determination of double bond positions. (A) Fatty acids are covalently modified by 1-(3-(aminomethyl)-4-iodophenyl)pyridin-1-ium (4-I-AMPP+) in an amidation reaction. (B) Photodissociation (PD) at 266 nm reveals the position of double bonds in unsaturated fatty acids. (B) Reprinted with permission from [67]. Copyright 2019 American Chemical Society.

was complemented by direct covalent attachment of the iodobenzoyl moiety to the amine.[71] Finally, crown ether derivatives enabled differentiation between isomeric glycans in lyso-glycosphingolipids that differ in a single stereocenter (epimers).[72] RDD of complexes containing either Glc or Gal yielded different fragment ion intensities, which allowed for relative quantitation of the epimers after calibration. Galactosyl- and glucosylceramides, which lack the primary amine, were distinguished by their differential reactivity towards iodophenyl boronic acid.

In a different approach, UV chromophores are selectively attached to double bonds in a Paternò-Büchi reaction to increase the UVPD efficiency and trigger double bond-specific fragmentation mechanisms.[73] The Paternò-Büchi reaction is a [2+2] photochemical reaction between a C=C and a C=O bond, which has been harnessed to pinpoint double bonds in unsaturated lipids.[74] UV irradiation of the ESI emitter tip containing the lipid and aldehyde or ketone triggers the formation of four-membered oxetanes, which are usually dissociated by CID. By using aryl ketones or aldehydes as derivatization agents, the absorption maximum of the modified lipids is redshifted into the range of solid-state UV lasers. 266 nm UVPD of phosphatidylcholines modified by acetophenone was found to double the selectivity towards the double bond location compared to CID.[73b] The increase in selectivity is explained by the local deposition of energy close to the double bond in the UVPD process. An additional advantage of UVPD over CID is that alkali metal-adducted Paternò-Büchi products are efficiently fragmented as well. On the contrary, non-modified lipids yielded no diagnostic fragments upon CID or 266 nm UVPD. In the following, the Paternò-Büchi reagent was further optimized to generate C=C diagnostic fragments with high yield.[73a] The most efficient reagent, 4-CF_3-benzophenone was employed in combination with wavelength-tunable UVPD to identify double bond isomers in glycerophospholipids from complex lipid extracts in a shotgun approach. The general scheme is shown in Figure 8. Overall, simple derivatization strategies can significantly increase the utility of UVPD for lipid analysis at different wavelengths.

3. Ultraviolet action spectroscopy

3.1. Action spectroscopy versus absorption spectroscopy

Photodissociation techniques including IRMPD and UVPD induce a change in *m/z* that can be detected by MS. Hence, the impact of irradiation on the ion, *i.e.*, an *action*, is measured. Recording photofragmentation spectra in a continuous wavelength range instead of a fixed wavelength yields a so-called action spectrum. Action spectroscopy is opposed to classical absorption spectroscopy, in which the light intensities before and after traversing a sample are compared (Figure 9). The light absorption is expressed in the Lambert-Beer law by the ratio between the transmitted light intensity I and the incident intensity I_0 at the light frequency ν as a function of the

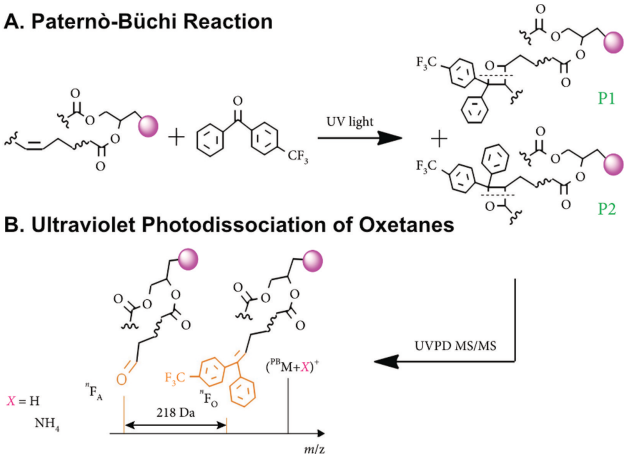

Figure 8. General scheme for Paternò-Büchi derivatization and ultraviolet photodissociation (UVPD) to pinpoint double bonds in glycerophospholipids. (A) C=C bonds in unsaturated glycerophospholipids are derivatized in a photochemical [2+2] Paternò-Büchi reaction with an aldehyde or ketone, here 4-CF_3-benzophenone. (B) Selective fragmentation of the resulting oxetanes by UVPD reveals the location of C=C bonds. Adapted from [73b]. Copyright 2022 Li et al. (Creative Commons Attribution 4.0 International License).

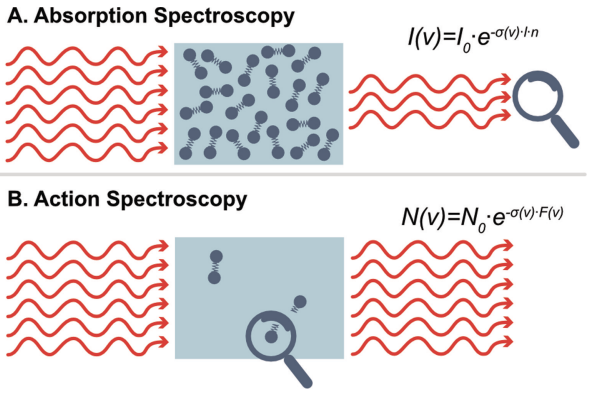

Figure 9. Comparison of the concepts underlying absorption and action spectroscopy. (A) Absorption spectroscopy requires a sufficient number density of analytes to induce a measurable light attenuation. (B) Action spectroscopy measures the effect of light absorption on the analytes. Adapted with permission from [14]. Copyright 2022 American Chemical Society.

absorption cross section $\sigma(v)$, path length l and number density n of the analyte (eq. 1).[75]

$$I(v) = I_0 \cdot e^{-\sigma(v) \cdot l \cdot n} \quad (1)$$

The prerequisite for absorption spectroscopy is a measurable attenuation of light intensity, which requires a sufficient number density of absorbing analytes in the range of 10^{10} cm^{-3} or more.[19] Hence, absorption spectroscopy is not applicable to ions in the gas phase, which are restricted by the space-charge-limit of 10^6 charges per cm^3.[19] The alternative is to measure the effect of irradiation on the ions by harnessing IRMPD, UVPD and other methods that induce detectable changes on the molecular level in response to light absorption. Assuming single photon absorption, such a process can be described by an equation equivalent to the Lamber-Beer law. It includes the number of ions N that remain unaffected upon irradiation at a specific light frequency v, the initial number of ions N_0, the absorption cross section $\sigma(v)$ and the photon fluence $\Phi(v)$ (eq. 2).[75]

$$N(v) = N_0 \cdot e^{-\sigma(v) \cdot \Phi(v)} \quad (2)$$

Action spectroscopy in the gas phase enables the investigation of single molecules or ions free from intermolecular interactions and solvent effects. Spectral broadening due to intermolecular interactions are thus eliminated and the spectral resolution can be further enhanced by cryogenic cooling, *e.g.* in cold ion traps.[7a,g,j] Optical transitions of isolated ions constitute molecular properties on a quantum mechanical level. Therefore, absorption frequencies are highly reproducible and can be predicted *in silico* by computational chemistry.[76] In the following, experimental approaches for action spectroscopy using UV and IR lasers are presented with a focus on applications and promises for lipid analysis. In order to unify the terminology employed for different action spectroscopy techniques, a comprehensive guideline was released recently.[77] According to these propositions, the techniques should be referred to under the generic term of *gas-phase action ion spectroscopy*, or simply *action spectroscopy* if the context is clear.

3.2. Ultraviolet photodissociation spectroscopy

UVPD spectroscopy monitors the wavelength-dependent photofragmentation induced by the absorption of UV photons.[17a] It has been mostly performed in ion traps coupled with tunable lasers such as optical parametric oscillators/amplifier (OPO/OPA) or dye lasers.[7d] Typically, UVPD spectra are recorded within the 200–400 nm (25000–50000 cm^{-1}) range. The electronic excitation energy is affected by the chemical environment of the UV chromophore and thus sensitive to the ion structure and conformation.[75] The interpretation of UV action spectra has benefitted from time-dependent density functional theory (DFT) and other quantum chemical approaches.[17a] Even though UV spectra become more challenging to compute with increasing molecular size due to complex vibronic transitions, UVPD spectroscopy is a valuable technique for molecular fingerprinting. UV spectra are particularly structured in the electronic band origins, which can be exploited to identify isobars or isomers that are indistinguishable by MS.[7j] UVPD spectroscopy has been applied to investigate various cations and anions ranging from metal complexes to biomolecules.[17a] Studies on lipids are rare, not least because they are mostly UV-inactive. Individual studies on lipids and some experimental approaches that can be relevant for future lipid analysis are presented in the following.

Coupling UVPD spectroscopy with MS combines the orthogonal information provided by each of the two techniques, which can be stored in databases and used for the quantitative identification of substances. In order to extract a maximum of structural information, a two-dimensional UV-MS setup was developed (Figure 10).[78] The experiment combines a cryogenic linear ion trap with an Orbitrap mass spectrometer. Following UV irradiation of the *m/z*-selected ions in the cold trap, the trap content is released and analyzed by MS. Hence, instead of measuring the overall fragmentation yield as a function of the UV wavelength, complete photofragmentation spectra are obtained at each wavelength of the UV laser. The result is a two-dimensional matrix containing the fragmentation yield as a function of both UV wavelength and *m/z*. With the help of such data arrays, isomers with very similar fragmentation mass spectra and small ion mobility differences can be distinguished.[78] An important condition, however, is vibrational resolution in the UV spectra, which requires cryogenic cooling.[7j] Due to increasing spectral broadening with increasing molecular size, the approach is best adapted to small- to midsize molecules including lipids and other metabolites.

Because most lipids except for those with delocalized pi systems do not absorb in the near-UV region, a chromophore must be attached.[79] A straightforward approach consists in the generation of non-covalent lipid-chromophore complexes in solution, which can be preserved during ESI. Aromatic amino

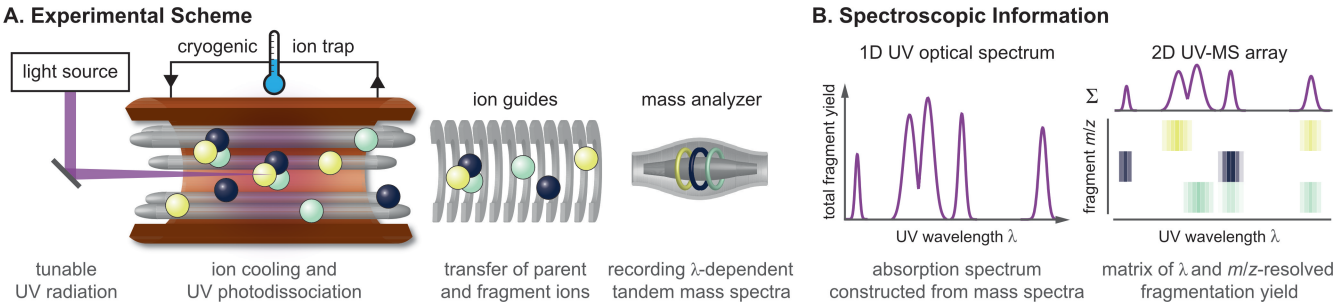

Figure 10. Principles and instrumentation for the 2D UV-MS technique described in [78]. (A) The instrument consists of a cryogenic ion trap with optical access coupled to an Orbitrap-based mass analyzer. (B) The UVPD spectrum and wavelength-dependent tandem mass spectra yield a two-dimensional matrix containing the fragmentation yield as a function of UV wavelength and *m/z*. Reprinted with permission from [14]. Copyright 2022 American Chemical Society.

acids and dipeptides were used as non-covalent, UV-active sensors to investigate several pairs of isomeric lipids in a cryogenic ion trap.[76] The non-covalent intermolecular interactions induce isomer-specific structural changes that can be detected by UVPD spectroscopy. Contrary to carbohydrates, for which all types of isomerism can be resolved by a single aromatic sensor (protonated tyrosine),[80] the structural diversity of lipids makes a one-fits-all approach illusory. Instead, preliminary computer simulations were performed to predict the most promising aromatic sensor for each pair of isomeric lipids. For steroids containing carbonyl and hydroxyl groups, protonated tyrosine yielded satisfying results owing to the formation of hydrogen bonding networks, similar to glycans (Figure 11A). In glycerophospholipids, however, the charged phosphate headgroup strongly binds the *N*-terminus of the aromatic sensor. Therefore, more flexible dipeptides were employed to promote additional interactions in the isomer-different domain of the lipid. Phenylalanine dipeptides enabled the distinction between PC *sn*-isomers via hydrogen-pi interactions with the hydrocarbon chains, contrary to the single amino acid (Figure 11B). Isomeric prostaglandins containing several oxygens were again best distinguishable by tyrosine-containing peptides, specifically alanine-tyrosine (Figure 11C). Finally, the quantification of isomers in binary mixtures was demonstrated for PC *sn*-isomers. By selecting only 7 isomer-specific wavelengths, the acquisition time was reduced by two orders of magnitude from 17 min to 14 s but the accuracy only slightly decreased from 3.3% to 3.7% root-mean-squared deviation (RMSD). The quantification of multi-component mixtures is more challenging, as demonstrated for a set containing up to five isomeric carbohydrates.[81] High accuracies of 3–5% RMSD were only achieved by scanning a continuous range instead of selected wavelengths. Overall, the use of lipid-aromatic complexes is a promising approach to render lipids UV-visible and to obtain isomer-specific UVPD spectra without time-consuming wet-chemical modification. The measurement of UVPD spectra at a few selected wavelengths renders the technique sufficiently fast for online coupling with LC–MS.[82] Though not yet demonstrated, mixing aromatic sensors with analytes could be induced between the LC column and ESI.[81] However, suitable sensors must be identified for each lipid class or possibly even for individual structures.

The reduction of acquisition times is a first step towards practical implementation of UVPD spectroscopy for analytical purposes. Further simplifications of the instrumentation, in particular ion trapping at elevated temperatures and the use of

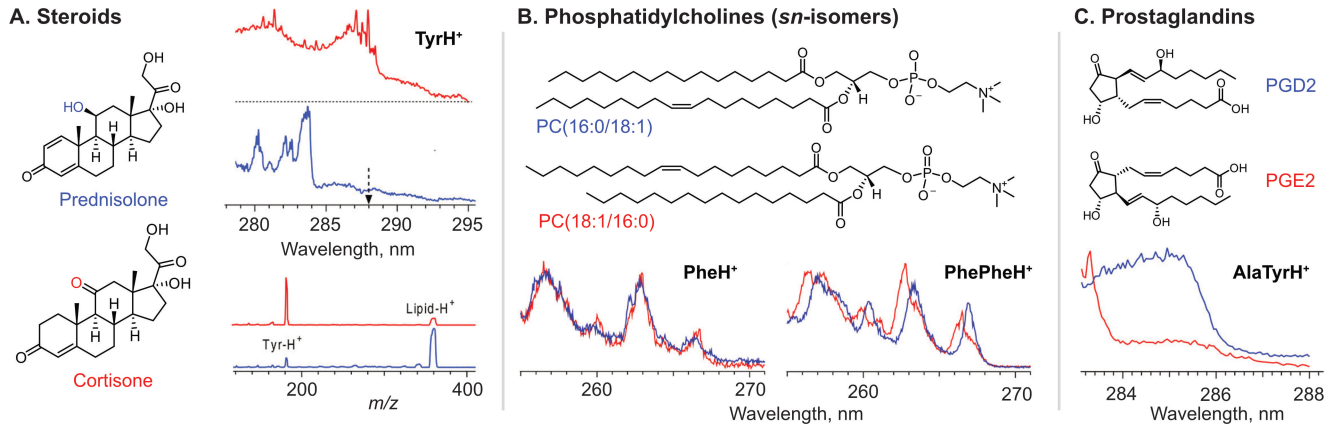

Figure 11. UVPD spectroscopy of isomeric lipids by non-covalent complex formation with aromatic amino acids and dipeptides. (A) Isomeric steroids are distinguishable by isomer-specific hydrogen bonds with protonated tyrosine. (B) The distinction of *sn*-isomers in glycerophospholipids requires more flexible phenylalanine-phenylalanine dipeptides to induce hydrogen-pi interactions in the isomer-different aliphatic domain. (C) Prostaglandins form hydrogen bonds with tyrosine in the alanine-tyrosine dipeptide. Adapted with permission from [76]. Copyright 2021 American Chemical Society.

a low-maintenance UV laser, were demonstrated on the example of the isomeric drugs ephedrine and pseudoephedrine.[83] The isomers are readily distinguishable and quantifiable by UVPD spectroscopy within seconds by measuring at three isomer-specific wavelengths. The accuracy of quantification was shown to be only slightly affected by rising the trapping temperature from 6 K to 64 K and simulating the typical line width of commercial mid-bandwidth UV OPOs of 5 cm^{-1} instead of 0.15 cm^{-1} achieved by high-resolution dye lasers. Elevated temperatures were shown to induce significant thermal broadening of vibronic transitions, which led to an overall decrease in the *s/n* by one order of magnitude. Nonetheless, using pressure-wave generators for cryogenic cooling to ~40 K instead of two-stage closed cycle refrigerators would largely facilitate the instrumentation.[84]

3.3. Variations of ultraviolet action spectroscopy

UV action spectroscopy does not necessarily have to rely on photofragmentation of ions and is amenable to modification with additional gas-phase techniques. For example, coupling a laser interaction region with IMS allows to obtain UV spectra of mobility-separated ions.[17a] DTIMS was hyphenated with UV action spectroscopy to study laser-induced photoisomerization and photodissociation of electrosprayed and mobility-separated molecular ions.[85] In a dual ion mobility setup, mobility-separated ions are irradiated with a tunable UV laser after traversing a first drift region. The resulting photoisomerization or photodissociation products are then separated in a second drift region and mass analyzed. When used to study photoisomerization, the detectable action is not photodissociation like in UVPD spectroscopy but a change in drift time. The setup can be employed to study *E/Z*-isomerization of C=C bonds in lipids, as demonstrated for several retinoid derivatives.[86] Retinoids are derived from vitamin A and belong to the category of prenol lipids. Retinal is the photoactive unit involved in the process of vision, where sub-picosecond *E/Z* photoisomerization triggers the visual transduction cascade.[87] The absorption maximum of retinal is highly dependent on its protein environment. To study the intrinsic absorption maxima of isolated retinal protonated Schiff base in the gas phase, photoisomerization of the all-*E* form to various *Z* forms was monitored as a function of the laser wavelength.[86a] Photofragmentation was found to be negligible at low laser intensities. In a subsequent study, photofragmentation was induced by applying significantly higher laser intensities in order to identify the structure of the major photofragment and propose a conclusive photofragmentation mechanism.[86c] Furthermore, a degradation product of retinal Schiff base was identified and shown to undergo reversible photo- and collision-induced *E/Z* isomerization in the gas phase.[86b] The effect of solvation on *E/Z* photoisomerization was investigated by comparing gas-phase and solution data of retinoic acid.[86d] In general, the combination of DTIMS and laser spectroscopy provides a powerful technique to study photoisomerizing molecules.

In addition to DTIMS, differential IMS (DIMS)[88] was coupled with UV action spectroscopy to separate and identify closely related species including conformers,[88a] protomers[88b] and isomers.[88c] Because conformational heterogeneity can cause spectral congestion even at cryogenic trapping temperatures, IMS is a valuable tool to obtain action spectra of individual conformers. A drawback observed in DIMS is that ions are energized due to the high electric fields, which can lead to interconversion of conformers.[88a] Nonetheless, the technique is interesting for the separation of lipid isomers with sufficiently high isomerization barriers. Especially ultra-high-resolution IMS techniques[89] hold a high potential for isomer-selective spectroscopy of lipids (see Section 4.2).

An alternative strategy to obtain isomer- and conformer-specific electronic spectra from a mixture is double-resonance UV-UV spectroscopy. The setup consists of a pump UV laser and a time-delayed probe UV laser, one of which operates at a fixed wavelength, whereas the second is scanned.[75] The fixed-wavelength laser is adjusted to a vibronic band of a specific isomer or conformer to deplete its ground-state population. This depletion is registered in the UV spectrum as an ion dip. In its first implementation, UV-UV spectroscopy was applied to neutral molecules in a supersonic jet expansion, which were detected by MS after photoionization.[90] Later, the application was extended to electrospray-generated ions in cold quadrupole ion traps.[91] Conformer-selective UV spectroscopy is difficult to apply to most lipids because of their large conformational flexibility. However, UV-UV spectroscopy has been used to study estrogen hormones, which belong to the category of sterol lipids and are comparably rigid due to their fused ring structure.[92] The conformational heterogeneity and hydrogen bonding was investigated in neutral estrogen molecules in a supersonic jet using fluorescence detection instead of MS. Individual conformers were identified, which were assigned to specific structures by comparison with DFT calculations. The estrogens were furthermore investigated by IR-UV double resonance spectroscopy (Section 4.2). It is important to note that quantification of conformers is not possible because the intensities also depend on the Franck-Condon factors.[7d]

In contrast to UVPD action spectroscopy, fundamentally different UV action spectroscopy schemes have been developed, which monitor other *actions* than covalent bond fragmentation: tagging spectroscopy and UV action spectroscopy in superfluid helium nanodroplets. Tagging photodissociation spectroscopy monitors the laser-induced dissociation of a weak ion-messenger complex and has been employed in the UV and adjacent visible range.[93] A weakly interacting tag is condensed onto the molecular ion, which is readily dissociated upon irradiation. However, tagging spectroscopy in the UV-vis range has gained much less importance than in the IR range (see Section 4.2). UV action spectroscopy in helium droplets allows for spectroscopy at ultimately cold temperatures. Ions are encapsulated in superfluid ^{4}He droplets with an intrinsic temperature of 0.37 K.[94] Irradiation of ions inside helium droplets does not lead to ion dissociation but induces evaporation of helium until the bare intact ion is released from the droplet in a nonthermal process.[95] Because only released

ions are detected by MS, background-free spectra are obtained. Electronic spectra of ions in helium droplets were first obtained for aniline molecules, which were ionized inside a TOF mass spectrometer by a crossing UV dye laser.[96] A second UV dye laser irradiating the ion-doped droplets with a delay of 200 ns induced the release of aniline ions from the droplets. A more universal approach using ESI for direct doping of helium droplets with *m/z*-selected ions was subsequently demonstrated.[97] Lipids have not been investigated by UV spectroscopy in helium droplets; however, the latter setup was later modified for IR spectroscopy of mass-selected biomolecular ions including lipids (see Section 4.3).

Chiral molecules can be studied by circular dichroism (CD) spectroscopy, which was only recently demonstrated for mass-resolved molecular ions.[98] Using circularly polarized UV light, CD spectra of electrospray-generated DNA polyanions[98a] and protonated amino acids[98b] were obtained by monitoring the electron photodetachment efficiency or UVPD yield, respectively. CD spectroscopy is particularly interesting for lipidomics because chirality plays an important role in lipid biochemistry.[99]

4. Infrared action spectroscopy

Typical IR action spectroscopy probes a continuous wavelength range in the mid-IR region and therefore only became widely applicable with the advent of sufficiently powerful, tunable IR lasers.[7e,l] IR spectroscopy is orthogonal to MS and provides essential structural information such as functional groups, symmetry, charged sites and hydrogen bonding networks.[7h] Being sensitive towards minute structural changes, the technique can identify closely related molecules including isomers and conformers by their spectroscopic fingerprints. Hyphenation of IR spectroscopy and MS thus combines the exceptional sensitivity and *m/z* selectivity of MS with the spectroscopic access to structural information. In recent years, the potential of IR action spectroscopy for studying metabolites[7h,8,100] and other small molecules of biological relevance[7b,k] has become more than evident. A range of different techniques have been developed to record IR spectra of *m/z*-selected ions, which can be divided into three categories: IRMPD spectroscopy, tagging photodissociation ion spectroscopy, and IR action spectroscopy in helium droplets (Figure 12).

The main difference between the three approaches lies in the action consequence of light absorption. In IRMPD spectroscopy, *m/z*-selected ions sequentially absorb multiple IR photons until the weakest bonds break and cause a detectable *m/z* shift. The fragment yield is plotted as a function of the wavenumber as an indirect measure for IR absorption. Whereas IRMPD spectroscopy is performed at room temperature, tagging photodissociation ion spectroscopy requires cryogenic temperatures to condense a weakly interacting tag (H_2, D_2, N_2 or noble gases) onto the *m/z*-selected ion. The neutral tag can be released in a single photon absorption event, often referred to as IR photodissociation (IRPD), in contrast to infrared multiple photon dissociation. Hence, an IR spectrum is obtained by measuring the wavelength-dependent ratio of untagged versus tagged ions. Helium droplet IR spectroscopy employs superfluid helium droplets as a cryogenic matrix (0.37 K)[101] to isolate *m/z*-selected ions. Irradiation of the ion-doped droplets with intense IR light triggers the release of bare ions from the droplets, which are detected by MS. Further details regarding instrumentation and physical processes underlying each technique are provided in the following sections.

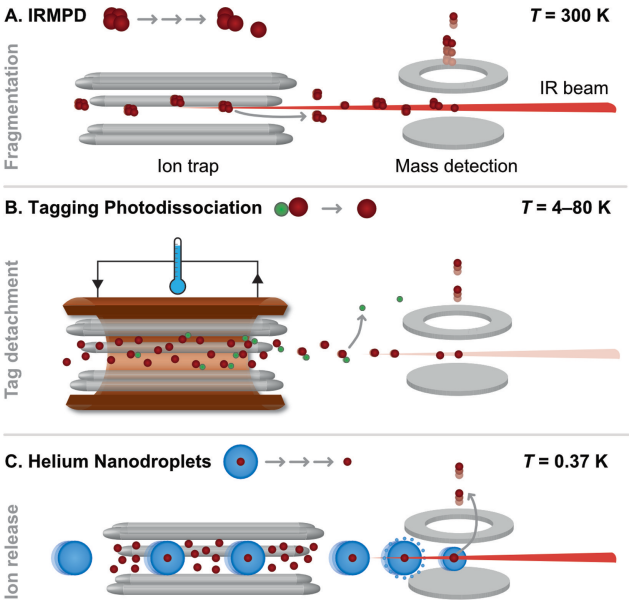

Figure 12. Experimental setups for gas-phase IR action spectroscopy. (A) Infrared multiple photon dissociation spectroscopy measures wavelength-dependent fragmentation. (B) Tagging photodissociation ion spectroscopy induces photodissociation of ion-messenger complexes. (C) IR action spectroscopy in helium droplets monitors the release of ions from helium droplets. All approaches involve the trapping of *m/z*-selected ions, spatial and temporal overlap between the ions and an IR beam, and detection of the action, *i.e.*, measuring the impact of the irradiation. Adapted with permission from [19]. Copyright 2022 American Chemical Society.

4.1. Infrared multiple photon dissociation spectroscopy

IRMPD spectroscopy monitors wavelength-dependent photofragmentation of ions, which is induced by the sequential absorption of multiple IR photons. The absorption and dissociation mechanisms underlying IRMPD were discussed in detail in Section 2.1. To obtain an IRMPD spectrum, the photofragmentation yield is plotted as a function of the wavenumber. The yield is defined as the cumulative intensity *I* of photofragments divided by the sum of precursor and fragment ion intensities (eq. 3).[102]

$$Yield = \frac{\sum I_{Fragment}}{\sum I_{Fragment} + I_{Precursor}} \quad (3)$$

IRMPD spectroscopy can be implemented in commercial mass spectrometers with minimal modifications to enable optical access, as was demonstrated for FTICR mass spectrometers and radio frequency-driven linear or 3D ion traps.[6e,7e,103]

The development of IRMPD spectroscopy was considerably fuelled by the emergence of IR free-electron lasers (FEL), which provide powerful, pulsed and continuously tunable radiation.[7e,g,i,19,103] Because the lasing wavelength of FELs is not defined by discrete transitions between quantum levels in an active medium but by the electron beam parameters and the machine design, FELs can reach any frequency in the mid-IR range that is interesting for IR action spectroscopy. Experiments that rely on FELs are tied to FEL facilities, which are publicly accessible in only a few institutions around the world. User facilities provide permanently installed spectrometers that can be used upon acceptance of a reasonable application, while more specialized equipment must be transported to this unique light source. The studies presented in this article were performed at one of the following FEL facilities: the Free Electron Laser for Infrared eXperiments (FELIX, Netherlands),[104] the Centre Laser Infrarouge d'Orsay (CLIO, France),[105] and the Fritz Haber Institute Free-Electron Laser (FHI FEL, Germany).[106] The most promising alternative tabletop lasers are solid state OPO/OPAs, which are pumped by high-power lasers such as Nd:YAG lasers or fiber lasers.[7h,107] However, the output of OPOs is usually not sufficiently intense to perform IRMPD spectroscopy in the 500–2000 cm^{-1} fingerprint region. Applications are thus restricted to the 3 μm (2500–4000 cm^{-1}) region, which contains informative hydrogen-stretching vibrations (CH, NH, OH).[7e,103] OPOs with high repetition rates (kHz-MHz) were shown to increase the photodissociation efficiency, especially in combination with decreased gas pressures in the ion trap.[103]

Disadvantages of IRMPD spectroscopy are redshifts of vibrational bands and the comparably broad bandwidth with full-width half-maximum (FWHM) values in the range of 10–50 cm^{-1}.[7e,h] Band broadening occurs mainly due to the population of higher vibrational states or conformations at elevated temperatures and complicates precise structural assignments. The main advantage of IRMPD spectroscopy over cryogenic spectroscopic methods is its straightforward integration into commercial MS platforms.[6e] As a consequence, IRMPD spectroscopy holds promise for the establishment of IR action spectroscopy as an analytical tool. Potential applications involve clinical, environmental or forensic analyses, in which sensitivity is a crucial parameter.[108] The ability of IRMPD spectroscopy to identify low-abundant lipids and other metabolites in complex organic mixtures such as body fluids and aerosols has been demonstrated repeatedly.[8,109] For example, isomeric oxidation products of the prenol lipid α-pinene were identified by IRMPD spectroscopy in secondary organic aerosols.[109c]

Even though studies employing IRMPD spectroscopy for lipid analysis are still scarce, many findings obtained for similarly sized metabolites will be beneficial for future lipid analysis. For example, the ability to distinguish substitution positions on aromatic rings is potentially interesting for the structural analysis of prenol lipids and polyketides that frequently contain substituted aromatic ring systems.[10] Substitution patterns on small aromatic molecules were indeed shown to yield distinguishable IR fingerprints.[110] In disubstituted phenyl rings, *ortho*-, *meta*- and *para* regioisomers were readily assigned based on diagnostic CH out-of-plane vibrations in the 650–900 cm^{-1} region.[110a] Surprisingly, these fingerprints are characteristic for the substitution position for a range of different analytes investigated as neutral, protonated, deprotonated or metal adducted species. This finding is very interesting in the context of drug discovery and metabolic transformation of drugs in the body, which often includes site-specific oxidation of aromatic rings.[110a] The technique was put into practice in a real-life example for the identification of novel psychoactive substances.[110b] Synthetic drugs are often designed based on a known molecular scaffold with only slight structural alterations such as the relative substitution positions on aromatic rings. Using IRMPD spectroscopy, regioisomeric fluoroamphetamines and methylmethcathinones were unambiguously distinguished and assigned using reference substances. For such small molecules, it is even feasible to assign unknown structures by matching the IR signature with computed spectra of candidate structures, as was demonstrated for a novel psychoactive substance detected in a confiscated street sample.

Structural assignment of unknown substances based on the match between the experimental spectrum and computed spectra of candidate structures opens up great opportunities because standards are not available in many cases. However, a reference-free approach based on computed spectra requires a reliable determination of the quality of the spectral match. For this purpose, an automated scoring procedure based on cosine similarity scores was recently developed, which allows for reference-free interpretation of IR spectra.[109b] However, this approach is to be applied with caution because computed harmonic IR spectra do not include anharmonicities that can lead to frequency shifts in the experimental spectrum. In addition, isomeric candidate structures often yield very similar spectra, thus causing ambiguity in the assignment. Even if complete structural assignment based on computed structures turns out to be impossible, the IR spectrum still yields functional group information that narrows down the number of eligible candidate structures.[7h,109a] The computational costs for computing IR spectra can be significantly reduced by machine learning approaches that employ either electronic- or nuclear structure-based models to predict vibrational spectra.[111] Even though current machine learning methods suffer from insufficient transferability to new systems, they have the potential to become a game changer for computational spectroscopy.

Several studies further suggest that it can be highly useful to record IR spectra of fragments in case the spectrum of the intact ion is too complex.[109a,110a] Due to the reduced size of the fragment ion, the complexity of its IR spectrum can be drastically reduced compared to the precursor by decreasing the number of oscillators and potentially the conformational flexibility. The gain in structural information by fragmentation was impressively demonstrated for the example of glutaric acid and ethylmalonic acid, which are isomeric biomarkers for inborn metabolic diseases and can be regarded as short-chain analogs of linear and branched fatty acids, respectively.[109a] The mere loss of a water molecule was shown to decrease the

spectral congestion tremendously (Figure 13). The fragment ion spectra furthermore provided an additional level of confidence in the assignment and distinction of glutaric and ethylmalonic acid. As illustrated in this example, fragment spectra can help in bottom-up identification of precursor structures, and their storage in databases will thus be an important step in identifying unknown structures.[109a,b]

In general, gas-phase IR action spectra are highly suitable for storage in databases to enable structural identification of unknown substances. However, a severe impediment to storing IRMPD spectra in databases is the non-linear dependence of band intensities on the laser pulse energy. Even though the positions of vibrational bands are highly reproducible on different instruments, intensity variations can complicate the comparison of spectra, especially if some bands vanish due to laser pulse energies below the dissociation threshold. Therefore, an automatic variable attenuator was recently developed to keep the FEL pulse energy constant.[102] Using the example of the lipid prostaglandin D2, the dependence of the IRMPD yield depending on the laser pulse energy was studied in detail, which revealed several pitfalls including low mass cutoff and electron detachment belying the actual fragmentation rate. The authors also concluded that using the fragment fluence (eq. 4) as the IRMPD intensity instead of the usually employed yield (eq. 3) holds the advantage that the spectra can be readily corrected for changes in the IR laser pulse energy and irradiation time.

$$Fragment\ fluence = -ln(1-Yield) \quad (4)$$

Another bottleneck on the way to the implementation of IRMPD spectroscopy into existing analytical workflows such as LC–MS is the acquisition time for an IRMPD spectrum, which is usually in the range of tens of minutes. LC peaks eluting typically within less than a minute can thus not be analyzed online in a straightforward manner. However, the integration of IR spectroscopy into LC–MS workflows is still highly desirable because chromatographic separation of complex mixtures can greatly simplify the spectroscopic analysis and enable to record isomer-pure IR spectra. Several strategies to obtain an LC–IR-MS hyphenation have recently been reported. One possibility to circumvent the time mismatch is to collect LC fractions and perform offline spectroscopic analyses of each fraction. Using this approach, isomeric metabolites of the drug atorvastatin were identified, which are separable by LC but unidentifiable based on their MS/MS spectra.[112] Furthermore, the technique was successfully applied to identify novel biomarkers in an untargeted metabolomics workflow.[113] Potential biomarkers were first identified by LC–MS of patient and control body fluids and then assigned to specific molecular structures by IRMPD spectroscopy of collected LC fractions.

Less time-consuming online LC–IR-MS workflows can be implemented by stopped-flow approaches and/or significant reduction of the spectroscopic acquisition time. The first online coupling of LC–MS with IRMPD spectroscopy was published in 2018 and applied to isomeric glycans.[114] The acquisition of isomer-pure IRMPD spectra was achieved by a stopped-flow strategy, which consists in reducing the flow rate significantly during spectroscopic analysis of eluting analytes. By decreasing the irradiation time per photofragmentation mass spectrum by almost 50% and only measuring a single mass spectrum at each datapoint instead of averaging three, the overall acquisition time for 1000 cm^{-1} was reduced from 45 min to 6.7 min. The emergence of kHz tabletop IR lasers is expected to further reduce the acquisition times and render the technology more interesting for analytical applications.[107] An IRMPD spectrum of protonated glucosamine was recorded within 14 s over a range of 1000 cm^{-1} by significantly reducing the irradiation time and number of datapoints. However, due to the low energy per pulse, state-of-the-art kHz IR lasers are only amenable to IRMPD spectroscopy of ions with low dissociation thresholds. Another idea that has been put forward for targeted identification of metabolites is to monitor the fragmentation yield only at a few diagnostic wavelengths, which is a particularly promising approach for high-resolution cryogenic IR spectroscopy.[115] However, if the IR spectra of isomers are sufficiently different, a targeted probing of single wavelengths is also feasible for IRMPD, as suggested for the isomeric prostaglandins E2 and D2.[7k] The identification of a pair of isomeric aromatic acids by online LC–IRMPD-MS with selective probing of a single wavelength was demonstrated recently.[7k] Prior knowledge of the whole IR spectrum is mandatory, which restricts the approach

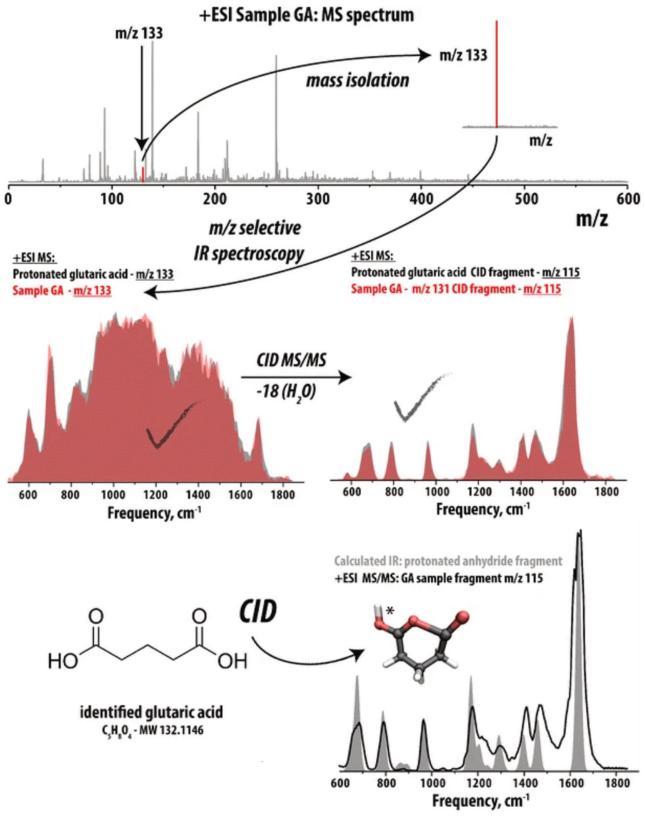

Figure 13. Identification of the biomarker glutaric acid in a body fluid and structure determination via reference samples and computation. Adapted from [109a]. Copyright 2018 Martens et al. (Creative Commons Attribution 4.0 International License).

to the identification of known substances. Furthermore, a quick-scan protocol was demonstrated, in which the FEL wavelength scans continuously over more than 500 cm^{-1} in less than a minute, which can be sufficient for an eluting LC peak.[7k]

Apart from chromatographic separation, purely gas-phase techniques have been employed to obtain isobar-, isomer- or even conformer-specific IRMPD spectra from mixtures: two-color IR spectroscopy and IMS. IR-IR spectroscopic approaches employ two independently tuned IR lasers and have one general prerequisite: a resolved, isomer- or conformer-specific transition. By fixing the first IR laser at the wavelength of that transition, the corresponding species gets depleted by fragmentation. The second IR laser is then scanned to obtain an IR spectrum of the remaining, *m/z*-selected ions in the ion trap. This approach is referred to as isomer-burning scheme. A recent study demonstrated that two-color IRMPD spectroscopy can be accomplished in a quadrupole ion trap with a single tunable laser instead of two separate light sources.[116] The technique was applied to identify novel psychoactive substances in a confiscated street sample that contained a mixture of isomeric 2- and 4-fluoromethamphetamine (Figure 14A). First, the IRMPD spectrum of the whole ion population was recorded. Then, an isomer population analysis was performed to determine whether multiple species are present and to identify isomer-specific transitions. Finally, one isomer was depleted and the IRMPD spectrum of the remaining isomer recorded. The IRMPD spectrum of the first isomer was obtained by subtracting the spectrum of the second isomer from the mixture spectrum. Even though a FEL was employed in that study, the approach in combination with a single table-top laser will render analytical applications very attractive. IR-IR photodissociation methods will be discussed further in the context of cryogenic IR ion spectroscopy.

The identification of an isomer- or conformer-specific transition for IR-IR spectroscopy is often challenging, especially with increasing molecular size and spectral congestion. An alternative is IMS, which provides post-ionization separation and yields orthogonal structural information. A major advantage of IMS over LC is the separation time, which occurs on the millisecond scale and therefore does not impose critical time constraints on the spectroscopic analysis. IMS has been successfully combined with IRMPD spectroscopy to study small metabolites. In a study combining DTIMS with IRMPD spectroscopy, protomers of benzocaine were mobility-separated and their respective IR spectra recorded (Figure 14B).[117] The baseline-separated drift peaks were assigned by comparison with DFT computed IR spectra to *O*- and *N*-protonated species, and their relative abundance was shown to depend on the solvent used for ESI. In another experimental setup, IRMPD spectroscopy was coupled with DIMS, which provides high-resolution separation, even though the mobility parameter cannot be directly linked to the ion structure like in DTIMS.[118] The setup was employed to study intramolecular interactions in isomeric metal-adducted monosaccharides. In a different study, DIMS was applied for the separation of the isomeric molecules

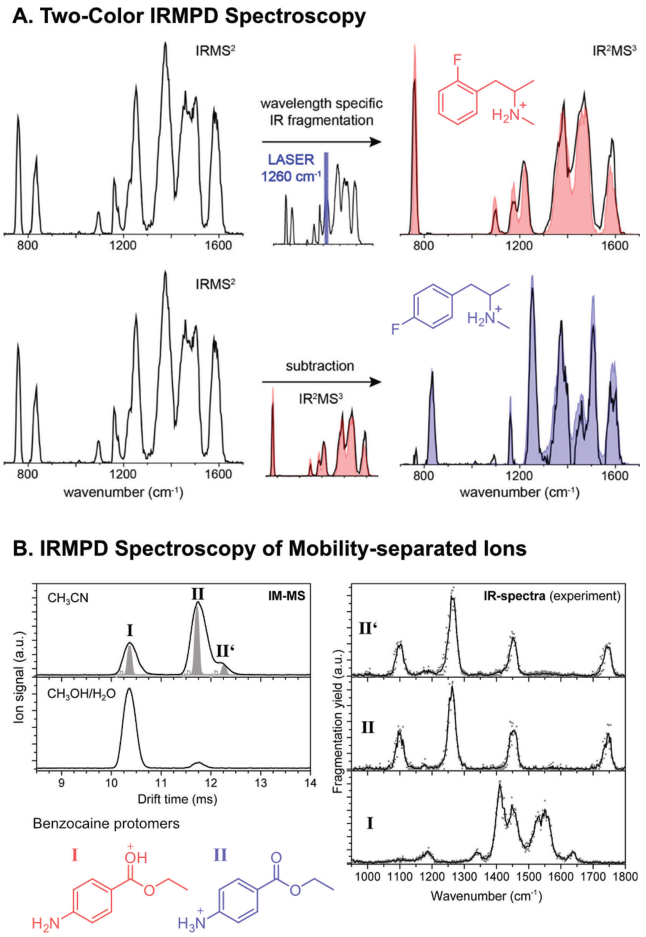

Figure 14. Isomer-specific IRMPD spectroscopy of small molecules using IR-IR spectroscopy (A) and drift tube ion mobility spectrometry (B). IRMPD spectra of isomeric fluoromethamphetamines were obtained by IR-IR spectroscopy. Protomers of benzocaine in different solvents were investigated by IRMPD spectroscopy after ion mobility separation. (A) Adapted from [116]. Copyright 2021 van Geenen et al. (Creative Commons Attribution Non-Commercial No Derivative Works 4.0 license). (B) Adapted from [117]. Copyright 2017 Warnke et al. (Creative Commons Attribution 4.0 International License).

paracetamol and 2-phenylglycine, which were assigned by comparison with IR spectra of reference standards.[119]

Taking one step apart from application-oriented research, IRMPD spectroscopy is also highly valuable in fundamental research. The technique can be employed to determine lipid fragment structures, which contribute to a more detailed understanding of lipid fragmentation mechanisms in MS/MS. For example, the structure of a diagnostic fragment formed upon dissociation of testosterone and related steroids was investigated by IRMPD spectroscopy.[120] Comparison with DFT computed spectra confirmed that the structure features a methyl-cyclopentenone ring instead of isomeric cyclohexanone, which helped to derive reasonable dissociation routes. Further, the fragmentation of glycerophospholipids and the impact of metal adduction on their gas-phase structures were recently investigated.[121] Glycerophospholipids constitute the most abundant lipid class in all mammalian membranes, and fundamental knowledge on their fragmentation in tandem MS

is thus of great interest.[122] To reduce complexity, the small model lipid PC(4:0/4:0) was chosen to investigate the impact of protonation, Na^+ and K^+ cationization on the three-dimensional gas-phase structures by IRMPD spectroscopy and DFT calculations.[121] The three-dimensional structures were then linked to experimentally observed fragmentation pathways. The major CID fragments resulting from neutral loss of phosphocholine from sodiated and potassiated PC were identified as dioxolane structures. Unfortunately, the results were ambiguous in the case of sodiated fragments. A higher spectral resolution offered by cryogenic IR ion spectroscopy can reduce such ambiguities, as shown in Section 4.3.[123]

4.2. Tagging photodissociation ion spectroscopy

The spectral congestion in IR action spectra can be significantly reduced by cryogenic cooling, which eliminates inhomogeneous broadening arising from thermally populated quantum states.[7g,j] By depopulating higher vibrational levels, the intensities of vibrational "hot" bands that do not originate from the vibrational ground state are substantially decreased. Spectral congestion arising from conformational heterogeneity can be reduced as well by annealing but oftentimes collisional cooling in cryogenic ion traps occurs sufficiently fast for kinetic trapping of higher-energy conformers.[7j]

Cryogenic action ion spectroscopy usually employs ion traps with optical access for ion collection, buffer gas cooling and irradiation. The most commonly used ion traps are radio frequency-driven linear traps composed of 4–22 poles or 3D Paul traps.[7j] Linear traps have a high trapping efficiency and capacity and offer the advantage that beam access and cooling below 10 K are straightforward. Initially employed 22-pole traps[124] were mostly replaced by lower-order linear traps that offer a lower effective storage volume but more stable radial confinement, which is crucial for spectroscopic applications.[7g] The advantages of linear ion traps were recently combined with the *m/z*-selectivity of Paul traps in the design of a cryogenic 2D linear ion trap, which thus incorporates all requirements for sensitive spectroscopy with MS/MS capabilities.[125] In tagging photodissociation ion spectroscopy, the trapped ions are tagged at cryogenic temperatures with messenger molecules or atoms of low polarizability in order to minimize their influence on the ionic structure. Typical messengers are chosen for their weak interactions, inertness and IR-transparency, with H_2, N_2, He and other noble gases being the most prominent examples. Because the non-covalent ion-messenger complexes are readily dissociated upon absorption of a single photon, action spectra that are equivalent to linear absorption spectra can be obtained by monitoring the depletion of the complex as a function of the wavenumber.[7f] A major advantage arising from the single-photon absorption process is that OPO lasers can be employed in the whole range (800–4000 cm^{-1}).[7d,e,126] Additionally, the use of a turn-key continuous-wave fiber-pumped laser in the 3 μm region was reported recently.[115]

Despite the high potential of tagging IR spectroscopy, lipids are yet underrepresented in this field of research. One study used hydrogen-tagging to investigate singly and doubly deprotonated dodecanedioic acid anions, which are dicarboxylate derivatives of 12:0 fatty acid.[127] DFT calculations showed that the H_2 tag induces only little perturbation of the molecular geometries and revealed an intramolecular hydrogen-bonded ring structure of the singly deprotonated ion. Another study was conducted on the drug valsartan and its metabolite, which share common structural motifs with lipids and fall into the same mass range.[128] Similar to the IRMPD study on atorvastatin metabolites,[112] this study showed that positional isomers of hydroxylated metabolites are readily distinguishable. In the case of hydroxylated valsartan, the natural metabolite and a synthetic regioisomer yielded highly resolved, separated O–H stretching vibrations in the 3 μm region. The distinction of hydroxylation and ring substitution isomers was also shown for smaller molecules by tagging IR spectroscopy[100] and is of high interest for the identification of drug metabolization in general. The functional groups of valsartan responsible for specific vibrational bands were identified by site specific isotopic substitution, and IR-IR double resonance spectroscopy was employed to probe the presence of multiple valsartan conformers. Interestingly, the spectrum of the hydroxylated metabolite was found to be simpler than that of valsartan itself because only one conformer is present. This observation shows that the spectral complexity does not universally increase with increasing molecule size but depends on the conformational flexibility as well.

Tagging spectroscopy offers a viable alternative to IRMPD spectroscopy.[100] Although it requires more complex instrumentation due to the need for cryogenic cooling, the single-photon absorption process needs less powerful light sources. Furthermore, comparison with computed IR spectra is more straightforward: anharmonic redshifts and band broadening observed in IRMPD spectroscopy are diminished, and the observed intensities are directly related to the absorption cross-sections and light intensity.[7c,g] Minor frequency shifts due to interactions with the messenger tag must, however, be taken into consideration when comparing experiment and theory.[7h] Tagging ion spectroscopy is unquestionably a promising approach to follow, especially to differentiate closely related molecules and structural details that remain unresolved in IRMPD spectroscopy. Furthermore, the technique enables multiplexed schemes, *i.e.*, recording of IR spectra of multiple analytes in parallel. Multiplexing is based on the fact that each tagged and untagged species can be related to each other by their mass difference, which corresponds to the known mass of the tag.[7h] Because tagging in cold ion traps is not 100% efficient, the obtained depletion spectra do not exhibit a zero baseline. This drawback can be overcome by solvent tagging, which is achieved by incomplete desolvation upon gentle nano-ESI.[84] The solvent-tagged ions are *m/z* selected in a quadrupole and interrogated by IR radiation, which releases the bare ions. Solvent tagging yields background-free IR spectra and enables relative isomer quantification with increased accuracy. Among other biomolecules, two diastereo-

meric sphingolipids tagged with 2-butanol were investigated and clearly distinguished in the 3 μm range.

For isomer- or conformer-selective cryogenic IR spectroscopy, IR-IR photodissociation schemes have been successfully implemented in several tagging IR spectroscopy setups.[129] In the isomer-burning method, the first IR laser irradiates *m/z*-selected ions at a fixed wavelength, followed by *m/z* selection of the non-dissociated ions, which are probed by the second, scanning IR laser. Alternatively, the first laser can be scanned and the second fixed at a specific wavelength, providing an ion-dip spectrum of the species with a transition at the fixed wavelength of the probe laser. Both methods are complementary, either burning away or selecting the ions absorbing at the wavelength of the fixed laser.[130]

IR-IR schemes in combination with cryogenic ion traps have been applied to obtain anomer- and conformer-specific IR spectra from monosaccharides including sodiated glucose[130] and protonated glucosamine.[131] By matching the IR spectra of specific conformers with computed spectra, further information on intramolecular H-bonding were obtained from diagnostic O–H stretching frequencies in the 3 μm region.[130–131] Furthermore, vibrations associated with the anomeric hydroxyl group were shown to be readily identifiable by ^{18}O isotopic labelling, which in turn yields an estimate on the number of conformers present.[131] More complex disaccharide anomers were investigated by IR-IR ion spectroscopy as well.[132] Two-color IR spectroscopy for the analysis of glycan isomers is particularly interesting in the context of glycolipids. As discussed further below, glycosphingolipids with stereoisomeric monosaccharide headgroups yield sharp, isomer-specific transitions in the 10 μm region, which makes them suitable candidates for IR-IR spectroscopy.[133]

Another conformer-selective technique that has been implemented in cold traps and should not remain unmentioned is IR-UV ion dip spectroscopy.[7e,j] In this technique, the UV laser is fixed at an electronic transition from the vibrational ground state of a specific conformer, whereas the preceding IR laser is scanned. Therefore, the UV dissociation yield drops if the IR laser is resonant with a vibrational transition, yielding a conformer-specific IR spectrum. The technique has been applied to biomolecules such as peptides, nucleotides and sugars but is less straightforward than IR-IR spectroscopy.[134] In particular, the IR-UV depletion technique necessitates a UV chromophore and a vibrationally resolved UV spectrum. The lack of chromophores and the high conformational flexibility of most lipids thus prevent the application of IR-UV ion dip spectroscopy in lipidomics, with a few exceptions such as sterol lipids.[92]

Even though lipids are understudied by tagging IR spectroscopy, some promising, innovative experimental setups have been reported that are very interesting for future lipid analysis. In particular, tagging spectroscopy was coupled with structures for lossless ion manipulation (SLIM) IMS.[132,135] SLIM is a type of TWIMS using pairs of electrodes on planar printed circuit boards that can be closely packed in space.[136] This ultra-high-resolution IMS technique[89] achieves long separation distances and resolving powers well-above 200[132,135] by multiple cycles. Cryogenic IR spectra of individual glycan anomers that differ in their CCS by as little as 0.2% were thus obtained.[135] The resolving power is sufficient for the separation of several kinds of lipid isomers such as double bond isomers in triglycerides and isomeric glycan headgroups in glycolipids (Figure 15).[137] Accurate CCS can be obtained on SLIM-based TWIMS platforms by employing a lipid class-dependent calibration strategy.[138] Previously, cryogenic IR spectroscopy was coupled with DTIMS for the analysis of glycans;[139] however, the resolution of DTIMS is insufficient to separate most lipid isomers.[137b]

The high resolution provided by SLIM finally rendered IMS competitive with IR-IR methods, the gold standard for isomer- and conformer-selective IR spectroscopy. As demonstrated on the example of disaccharide anomers, very similar spectra were obtained using either IR-IR double resonance with helium tagging or SLIM IMS with nitrogen tagging.[132] The anomeric configuration of larger glycans was determined by mobility-selective CID and cryogenic IR spectroscopy of reducing-end fragments, thus requiring only a small library of anomerically pure mono- and disaccharide standards to assign anomers.[140] The potential of SLIM IMS coupled with tagging IR spectroscopy as a high-throughput analytical technique has been impressively demonstrated by a recently developed instrument.[115] It allows to push acquisition times to a few minutes or even down to seconds by multiplexing and relies on a user friendly turn-key fiber-pumped IR laser. The

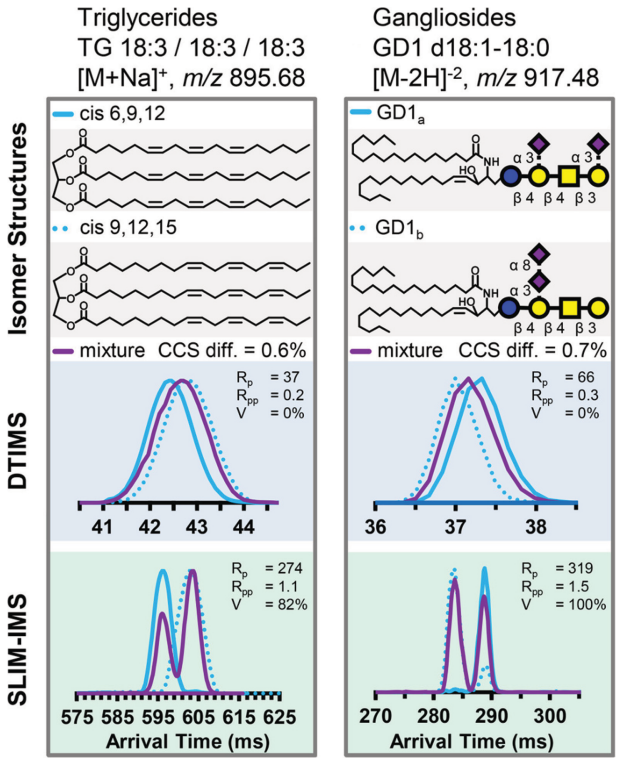

Figure 15. Separation of lipid isomers by structures for lossless ion manipulation (SLIM). Double bond isomers in triglycerides and glycan isomers in gangliosides were separated by ultra-high-resolution ion mobility spectrometry but not by classical drift tube ion mobility spectrometry (DTIMS). Adapted with permission from [137b]. Copyright 2021 American Society for Mass Spectrometry.

implementation of a multiplexed technique based on Hadamard transform was demonstrated to increase the *s/n* and enable fast spectroscopic analysis of mobility-separated species in complex mixtures in a single laser scan.[141] Hyphenating SLIM IMS with tagging IR spectroscopy hence constitutes a fast and powerful single-laser alternative to IR-IR double resonance methods.

4.3. Infrared action spectroscopy in helium droplets

A variation of cryogenic IR action ion spectroscopy is IR spectroscopy in helium droplets.[142] In this technique, ions are embedded in superfluid ^{4}He droplets, which can be regarded as IR-transparent isothermal (0.37 K) cryostats for the encapsulated analyte. Below 2.17 K, ^{4}He is superfluid and exhibits a vanishingly small viscosity.[101] Therefore, the helium matrix does not influence the intrinsic vibrations of the ion, contrary to the tags employed in tagging ion spectroscopy. IR action spectroscopy in helium droplets was initially developed for neutral molecules.[142] Spectroscopy of ions in superfluid helium droplets was first achieved by laser-induced ionization of the analyte inside the mass spectrometer.[143] Shortly after, the coupling of helium droplet spectroscopy with ESI rendered the technique universally applicable to all kinds of biomolecules.[97a,144]

In the first experimental setup developed for IR spectroscopy of electrospray-generated biomolecular ions, superfluid helium droplets pick up ions from a linear ion trap and carry them to the interaction region.[97a] The sequential absorption of multiple IR photons by the ion inside the droplet leads to the evaporation of helium until the bare ion is released from the droplet and detected by MS. Importantly, only released ions but no helium-tagged ions are detected in the mass spectrometer, which yields zero-baseline spectra. Because IR action spectroscopy in helium droplets involves a multiple photon absorption process, the intensities do not scale linearly with the laser pulse energy. Furthermore, the technique relies on the high photon flux provided by FELs.[97a,145] The need for cryogenic cooling and the generation of helium droplets requires complex and expensive instrumentation, which restricts applications to fundamental research. The strength of helium droplet spectroscopy lies in the background-free recording of ultra-high-resolution IR spectra at ultimately cold temperatures.

The performance of helium droplet spectroscopy in lipid analysis has been investigated in several studies focusing on different lipid classes and their respective isomers. An important field of research is concerned with the investigation of lipid fragmentation mechanisms in MS/MS. For example, glycerolipids undergo abundant neutral loss of the phosphate-containing headgroup, as discussed in Section 4.1. A seminal work from 2003 suggested that the fragmentation is accompanied by cyclization of the glycerol backbone.[146] However, two different mechanisms yielding two different products are imaginable (Figure 16A): Participation of the fatty acid at the *sn*-2 position yields dioxolane fragments, whereas dioxane

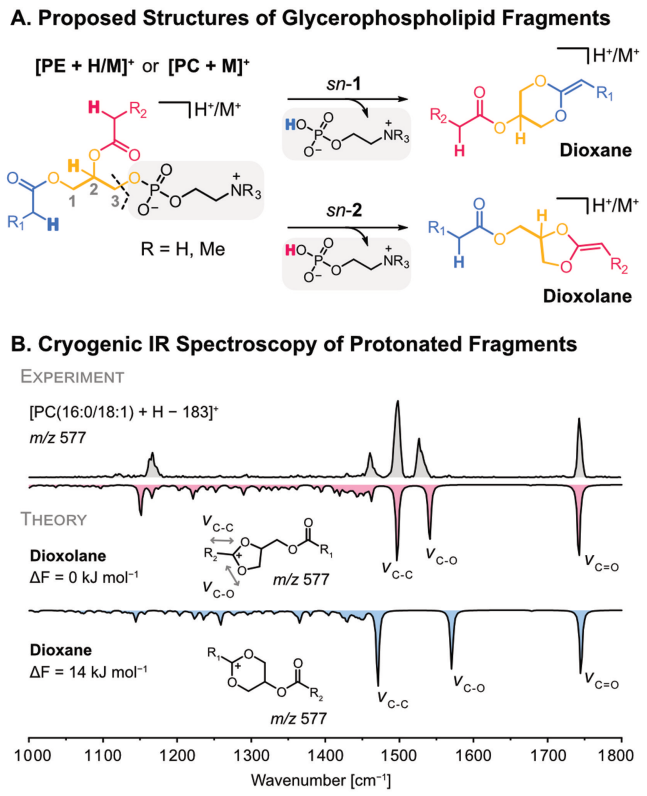

Figure 16. Investigation of glycerolipid fragmentation by high-resolution IR action spectroscopy in helium droplets. (A) Two hypothetical dissociation mechanisms yield dioxane or dioxolane fragments, respectively. (B) The formation of dioxolane fragments was confirmed by IR action spectroscopy. Adapted from [123]. Copyright 2021 Kirschbaum et al. (Creative Commons Attribution 4.0 International License).

fragments are formed by *sn*-1 participation. The IRMPD spectra of alkali metal adducts yielded partially ambiguous assignments due to the broadness of bands and similarity between computed dioxolane and dioxane spectra.[121] IR spectra of protonated fragments obtained by helium droplet spectroscopy, on the contrary, enabled clear assignment of the dioxolane structure and the corresponding fragmentation mechanism (Figure 16B).[123] In a different study, the same fragments were investigated as silver adducts by helium droplet spectroscopy.[147] IR spectroscopy was employed in this case to explain previously observed, isomer-specific MS^3 fragmentation of silver-adducted glycerolipids. The results show that the silver coordination geometry in the MS^2 dioxolane fragments determine the ion abundances in MS^3 spectra. The silver coordination geometry is, in turn, influenced by the *sn*-position of the fatty acids and by C=C bond positions within the fatty acids. Thus, isomer-specific ion intensities in MS^3 spectra were rationalized by investigating three-dimensional ion structures with high-resolution IR spectroscopy.

Helium droplet IR spectroscopy is also suitable to resolve minute structural details in isomeric lipids. In this context, double bond regio- and stereoisomers in sphingolipids[148] and fatty acids[149] were investigated, which only differ in the position or geometry of a C=C bond. Sphingolipids contain an amino alcohol, which is protonated upon ESI. The protonated

amine can act as a double bond sensor by interacting with the electron-rich C=C bond in the lipid chain.[150] Depending on the C=C location, the overall geometry of the intramolecular interaction and thus the IR spectrum are affected. Hence, differences in the IR spectra of C=C regio- and stereoisomers in 1-deoxysphingolipids were observed by high-resolution IR spectroscopy (Figure 17).[148] Furthermore, hydroxylation regioisomers of 1-deoxysphingolipids were shown to yield distinguishable fingerprints. Fatty acids, on the contrary, do not contain a basic functional group that can act as an intrinsic double bond sensor upon protonation. Therefore, ammonium and alkylamines were tested as extrinsic double bond sensors for IR spectroscopy.[149] Non-covalent complexes were readily formed during ESI but, contrary to the complexation of lipids with aromatic amino acids used to distinguish isomers by UVPD spectroscopy,[76] the gain in structural information was rather limited. Covalent modification of fatty acids is a promising alternative because the conformation of the molecule is expected to be more rigid.

Another type of lipid isomers that have been investigated by helium droplet spectroscopy are glycolipids.[133] Isomeric glycosphingolipids bearing mono- or trisaccharides were found to yield highly diagnostic fingerprints in the spectral region from 1000–1150 cm^{-1}. Furthermore, it was possible to deconvolve IR spectra of isomeric mixtures using reference spectra and non-negative matrix factorization. In good agreement with a study on human milk oligosaccharides,[151] the limit of detection for individual isomers was determined to be $<5\%$. Provided that isomer-specific transitions are sufficiently well-resolved, deconvolution of mixture spectra is thus an alternative to IR-IR ion spectroscopy or IMS for the analysis of isomeric mixtures. Finally, glycolipid isomers extracted from mouse cells were identified, which demonstrates that the approach is suitable for biological applications that are hampered by low sample amounts. Contrary to nuclear magnetic resonance (NMR) spectroscopy, the sample does not need to be highly purified for IR action spectroscopy.

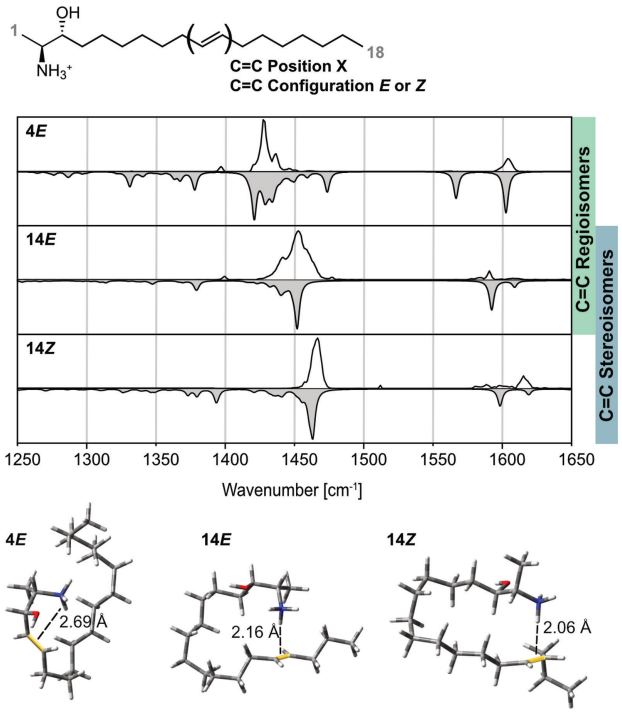

Figure 17. Identification of C=C regio- and stereoisomers in 1-deoxysphingolipids by IR action spectroscopy in helium droplets. Charge-olefin interactions between the protonated amine and the C=C bond result in diagnostic N–H bending frequencies. Inverted gray traces are computed harmonic IR spectra corresponding to the experimental spectra. Adapted from [148]. Copyright 2020 Kirschbaum et al. (Creative Commons Attribution 4.0 International License).

5. Challenges and perspectives

Even though photodissociation and action spectroscopy have proven enormous potential for lipidomics, they are not yet routinely employed. Several key factors impede their widespread application, which are in the focus of ongoing research.

Instrumentation: The large majority of mass spectrometers capable of photodissociation or action spectroscopy presented herein are custom-built instruments in specialized laboratories. The only exceptions are FTICR platforms with integrated IRMPD[21] and recently introduced Orbitrap systems equipped with UVPD.[37] The added value of IRMPD for lipid analysis is limited, whereas commercial UVPD holds great promises for future lipidomic applications (*cf.* Sections 2.2 and 2.3).[6b,c] Although commercial solid-state UV lasers operate at longer wavelengths (213 or 266 nm) than 193 nm excimer lasers, 213 nm UVPD was shown to constitute a viable alternative for lipid analysis.[37] Furthermore, tailor-made UV chromophores make the 266 nm range accessible to lipids and trigger alternative fragmentation pathways.[64,73b]

In addition, IRMPD spectroscopy provides a significant increase in structural information compared with fixed-wavelength IRMPD. Even though the spectral resolution at room temperature is limited, the technique is relatively straightforward to implement in commercial mass spectrometers.[6e] Due to its simplicity, IRMPD spectroscopy has the potential to be established as an orthogonal technique in clinical laboratories to identify predefined metabolites[8,109a] or novel biomarkers[113] in patient samples.[108] In contrast, cryogenic IR and UV action spectroscopy require additional instrumentation for cryogenic cooling and are not ready for commercialization yet. Efforts towards performing UVPD spectroscopy at elevated temperatures to avoid helium cooling lead to a reduction in *s/n* by one order of magnitude, which may be deleterious for several applications.[83] For now, the particular strength of cryogenic action spectroscopy lies in fundamental research such as investigating lipid fragmentation mechanisms at high spectral resolution.[123]

Light sources: For UVPD, several alternative light sources including 255, 265, and 275 nm light emitting diodes (LEDs),[152] extreme-UV (40–80 nm) gas-discharge lamps[153] and vacuum-UV (115–160 nm) deuterium lamps[154] have been investigated. Such lower-cost and user-friendly light sources can replace lasers in some applications and are expected to boost the widespread use of UVPD.[6c]

The future of IR and UV action spectroscopy is largely driven by current advancements in laser technology. To be established as an analytical technique, IR action spectroscopy must become independent from FELs and adopt solid-state table-top solutions.[155] Alternative mid-IR light sources are OPOs,[103] semiconductor-based quantum cascade lasers[156] and hybrid fiber-bulk chalcogenides based laser systems.[157] OPOs provide high intensities in a relatively large tuning range, and especially kHz and MHz OPOs were shown to provide high quality IRMPD spectra in the 3 μm range.[103,107] Also for UV action spectroscopy, UV OPOs can be an attractive alternative to high-maintenance UV dye lasers despite their increased FWHM.[83] In tagging IR photodissociation ion spectroscopy, OPOs are already routinely used.[132,135] The output in the mid-IR range of $AgGaSe_2$ crystals (800–2100 cm^{-1}) is sufficient to induce fragmentation of a significant fraction of ions, rendering the entire molecular fingerprint range (800–4000 cm^{-1}) accessible by OPO systems.[7d,126] Furthermore, a large tuning range might no longer be necessary for targeted screening of database-stored compounds at a few selected wavelengths because full-range IR spectra of metabolites recorded using FELs are increasingly made available in databases.[7k]

A disadvantage of OPO lasers is that they require some expertise to tune and often do not have an optimal focus and beam profile. Turn-key fiber-pumped lasers are therefore a promising alternative for future applications. They are easy to use, compact and provide a sufficient photon flux for tagging photodissociation IR spectroscopy. These advantages were recently demonstrated by integrating a fiber-pumped laser operating in the 3 μm range in continuous wave mode in a high-throughput instrument.[115]

Acquisition times: Acquisition times are a crucial parameter of all MS/MS and spectroscopic techniques. Coupling photodissociation and action spectroscopy with LC–MS workflows is required to study complex lipid extracts. Unlike many lamp-based UVPD approaches,[153–154] laser-based UVPD occurs on very short timescales and is readily compatible with high-throughput LC–MS.[6c] On the contrary, acquisition times are a substantial bottleneck in action spectroscopy. Scanning a wavelength range of 1000 cm^{-1} with a FEL requires up to 45 min.[107] However, online coupling of IRMPD spectroscopy with LC–MS is possible by stopped-flow approaches in combination with reduced irradiation times[114] or measuring a reduced number of datapoints using kHz laser technology.[107] The reduction of datapoints is driven to the extreme by selecting only one or a few wavelengths.[7k,76,82–83] Measuring at a single wavelength enabled to assign LC-separated peaks of isomers in an online workflow.[7k] However, this approach is only applicable to known substances in targeted analyses. Most recently, rapid acquisition of an IRMPD spectrum over a >600 cm^{-1} range in less than a minute was demonstrated by continuous instead of stepped FEL scanning.[7k] A major advantage of tagging photodissociation spectroscopy in terms of acquisition time is the possibility to perform multiplexed analyses.[115,141] Several species can be tagged and detected simultaneously, which leads to an overall improved duty cycle. IR fingerprints of mobility-separated ions were recorded over a range of 450 cm^{-1} within a few seconds to minutes.[115]

Data interpretation: Compared to CID and IRMPD, UVPD spectra are often exceedingly complex. Extensive fragmentation provides increased structural information but also implies difficult data interpretation. Automated approaches for data collection and analysis were established for lipid A[48h,i] but for the most part, data interpretation is manual work.[48i] UVPD enables *de novo* identification of lipids, whereas spectroscopic approaches require either computed or experimental reference spectra for structural assignment. In contrast to photodissociation spectra, IR and UV action spectra can be predicted by quantum chemistry, which allowed for reference-free assignment of IR spectra to specific structures.[7k,109b] However, the identification of unknown substances is not trivial because of large numbers of possible isomeric candidate structures.[7h] The increasing spectral congestion with growing molecule size imposes a mass limit, for example for complex lipooligosaccharides. In some cases, this bottleneck can be overcome by fragmentation.

6. Conclusion

Photodissociation and action spectroscopy are invaluable tools for in-depth lipid analysis. Coupling laser light with MS can yield insights into structural details that are difficult to access by other analytical techniques. In the past years, UVPD has aided the *de novo* structural identification of lipids in high-throughput LC–MS workflows. Fixed-wavelength IRMPD yields less informative fragments but becomes an exceedingly powerful tool when extended to a continuous spectral range: IR action spectroscopy synergizes the sensitivity and mass-selectivity of MS with the diagnostic potential of IR spectroscopy. Their combination provides significant advantages over condensed-phase analytical techniques such as NMR spectroscopy in terms of the required sample concentration and purity. IR action spectroscopy is therefore highly attractive in a clinical context, *e.g.* for biomarker identification directly from patient fluids. IR action spectra generally contain more diagnostic features and are more readily predictable than UV action spectra. In addition, lipids generally do not contain chromophores, which makes the design of lipid-specific UV chromophores necessary. Future lipid analysis is therefore expected to benefit especially from fixed-wavelength UVPD and IR action spectroscopy. The key bottlenecks are sophisticated instrumentation, insufficient sensitivity for real life applications and low duty cycles. However, continuous progress in all directions is currently being observed. Eventually, IR action spectroscopy might enable not only the identification of isolated lipids but also of lipids assembled in complex biological conjugates. For example, the identity of membrane protein-bound lipids could be determined by using hybrid ion activation techniques to dissociate the lipid from the protein-lipid complex prior to detailed structural identification of the released lipid by action spectroscopy. Thus, interactions between lipids and pharmaceutically highly relevant GPCRs

could be uncovered by the powerful couple formed by MS and laser light, with the ultimate aim to develop novel therapeutical approaches.

Acknowledgements

The authors acknowledge generous funding by the European Research Council, ERC-2019-CoG-863934-GlycoSpec. C.K. thanks the Fonds der Chemischen Industrie for financial support. Open Access funding enabled and organized by Projekt DEAL.

Conflict of Interest

The authors report no conflict of interest.

Data Availability Statement

Data sharing is not applicable to this article as no new data were created or analyzed in this study.

Keywords: Action spectroscopy · Laser · Lipids · Mass spectrometry · Photodissociation

[1] N. D. Ridgway, R. S. McLeod, *Biochemistry of Lipids, Lipoproteins and Membranes*, 6th Edition, Elsevier, Amsterdam, **2016**.
[2] S. E. Hancock, B. L. Poad, A. Batarseh, S. K. Abbott, T. W. Mitchell, *Anal. Biochem.* **2017**, *524*, 45–55.
[3] a) Y. H. Rustam, G. E. Reid, *Anal. Chem.* **2018**, *90*, 374–397; b) J. R. Bonney, B. M. Prentice, *Anal. Chem.* **2021**, *93*, 6311–6322; c) W. Zhang, R. Jian, J. Zhao, Y. Liu, Y. Xia, *J. Lipid Res.* **2022**, *63*, 100219.
[4] a) S. J. Blanksby, T. W. Mitchell, *Annu. Rev. Anal. Chem.* **2010**, *3*, 433–465; b) S. Heiles, *Anal. Bioanal. Chem.* **2021**, *413*, 5927–5948.
[5] a) E. Ryan, G. E. Reid, *Acc. Chem. Res.* **2016**, *49*, 1596–1604; b) T. Porta Siegel, K. Ekroos, S. R. Ellis, *Angew. Chem. Int. Ed.* **2019**, *58*, 6492–6501; *Angew. Chem.* **2019**, *131*, 6560–6569; c) S. Cheng, X. Zhao, X. Ma, in *Advanced Fragmentation Methods in Biomolecular Mass Spectrometry, Vol. 9* (Ed.: F. Lermyte), Royal Society of Chemistry, Cambridge, **2020**, pp. 209–234; d) F. Xia, J. B. Wan, *Mass Spectrom. Rev.* **2021**, e21729; e) A. Bednařík, V. Prysiazhnyi, D. Bezdeková, J. Soltwisch, K. Dreisewerd, J. Preisler, *Anal. Chem.* **2022**, *94*, 4889–4900.
[6] a) J. P. Reilly, *Mass Spectrom. Rev.* **2009**, *28*, 425–447; b) J. S. Brodbelt, *Chem. Soc. Rev.* **2014**, *43*, 2757–2783; c) J. S. Brodbelt, L. J. Morrison, I. Santos, *Chem. Rev.* **2020**, *120*, 3328–3380; d) J. S. Brodbelt, J. J. Wilson, *Mass Spectrom. Rev.* **2009**, *28*, 390–424; e) J. R. Eyler, *Mass Spectrom. Rev.* **2009**, *28*, 448–467.
[7] a) T. R. Rizzo, J. A. Stearns, O. V. Boyarkin, *Int. Rev. Phys. Chem.* **2009**, *28*, 481–515; b) N. C. Polfer, J. Oomens, *Mass Spectrom. Rev.* **2009**, *28*, 468–494; c) N. C. Polfer, *Chem. Soc. Rev.* **2011**, *40*, 2211–2221; d) N. C. Polfer, P. Dugourd, *Laser Photodissociation and Spectroscopy of Mass-separated Biomolecular Ions, Vol. 83*, Springer, Cham, **2013**; e) C. N. Stedwell, J. F. Galindo, A. E. Roitberg, N. C. Polfer, *Annu. Rev. Anal. Chem.* **2013**, *6*, 267–285; f) A. B. Wolk, C. M. Leavitt, E. Garand, M. A. Johnson, *Acc. Chem. Res.* **2014**, *47*, 202–210; g) T. R. Rizzo, O. V. Boyarkin, *Top. Curr. Chem.* **2015**, *364*, 43–97; h) A. P. Cismesia, L. S. Bailey, M. R. Bell, L. F. Tesler, N. C. Polfer, *J. Am. Soc. Mass Spectrom.* **2016**, *27*, 757–766; i) L. Jašíková, J. Roithová, *Chem. Eur. J.* **2018**, *24*, 3374–3390; j) O. V. Boyarkin, *Int. Rev. Phys. Chem.* **2018**, *37*, 559–606; k) J. Martens, R. E. van Outersterp, R. J. Vreeken, F. Cuyckens, K. L. M. Coene, U. F. Engelke, L. A. J. Kluijtmans, R. A. Wevers, L. M. C. Buydens, B. Redlich, G. Berden, J. Oomens, *Anal. Chim. Acta* **2020**, *1093*, 1–15; l) T. L. Guasco, M. A. Johnson, in *Emerging Trends in Chemical Applications of Lasers, Vol. 1398* (Eds.: M. R. Berman, L. Young, H.-L. Dai), ACS Publications, Washington, D. C., **2021**, pp. 277–306.
[8] J. Martens, G. Berden, R. E. van Outersterp, L. A. J. Kluijtmans, U. F. Engelke, C. D. M. van Karnebeek, R. A. Wevers, J. Oomens, *Sci. Rep.* **2017**, *7*, 3363.
[9] D. A. Bender, S. P. Datta, A. D. Smith, *Oxford Dictionary of Biochemistry and Molecular Biology*, 2nd Edition, Oxford University Press, Oxford, **2000**.
[10] E. Fahy, S. Subramaniam, H. A. Brown, C. K. Glass, A. H. Merrill, R. C. Murphy, C. R. Raetz, D. W. Russell, Y. Seyama, W. Shaw, T. Shimizu, F. Spener, G. van Meer, M. S. VanNieuwenhze, S. H. White, J. L. Witztum, E. A. Dennis, *J. Lipid Res.* **2005**, *46*, 839–861.
[11] M. Sud, E. Fahy, D. Cotter, A. Brown, E. A. Dennis, C. K. Glass, A. H. Merrill, R. C. Murphy, C. R. Raetz, D. W. Russell, S. Subramaniam, *Nucleic Acids Res.* **2007**, *35*, D527–532.
[12] a) E. Fahy, S. Subramaniam, R. C. Murphy, M. Nishijima, C. R. Raetz, T. Shimizu, F. Spener, G. van Meer, M. J. Wakelam, E. A. Dennis, *J. Lipid Res.* **2009**, *50*, S9–14; b) G. Liebisch, E. Fahy, J. Aoki, E. A. Dennis, T. Durand, C. S. Ejsing, M. Fedorova, I. Feussner, W. J. Griffiths, H. Köfeler, A. H. Merrill, R. C. Murphy, V. B. O'Donnell, O. Oskolkova, S. Subramaniam, M. J. O. Wakelam, F. Spener, *J. Lipid Res.* **2020**, *61*, 1539–1555; c) V. B. O'Donnell, E. A. Dennis, M. J. O. Wakelam, S. Subramaniam, *Sci. Signaling* **2019**, *12*.
[13] a) G. Liebisch, K. Ekroos, M. Hermansson, C. S. Ejsing, *Biochim. Biophys. Acta Mol. Cell Biol. Lipids* **2017**, *1862*, 747–751; b) J. P. Koelmel, C. Z. Ulmer, C. M. Jones, R. A. Yost, J. A. Bowden, *Biochim. Biophys. Acta Mol. Cell Biol. Lipids* **2017**, *1862*, 766–770; c) L. S. I. Consortium, *Nat. Metab.* **2019**, *1*, 745–747; d) H. C. Köfeler, R. Ahrends, E. S. Baker, K. Ekroos, X. Han, N. Hoffmann, M. Holcapek, M. R. Wenk, G. Liebisch, *J. Lipid Res.* **2021**, *62*, 100138; e) G. Liebisch, J. A. Vizcaino, H. Köfeler, M. Trotzmuller, W. J. Griffiths, G. Schmitz, F. Spener, M. J. O. Wakelam, *J. Lipid Res.* **2013**, *54*, 1523–1530.
[14] M. Grabarics, M. Lettow, C. Kirschbaum, K. Greis, C. Manz, K. Pagel, *Chem. Rev.* **2022**, *122*, 7840–7908.
[15] D. Kopczynski, N. Hoffmann, B. Peng, G. Liebisch, F. Spener, R. Ahrends, *Anal. Chem.* **2022**, *94*, 6097–6101.
[16] J. G. McDonald, C. S. Ejsing, D. Kopczynski, M. Holcapek, J. Aoki, M. Arita, M. Arita, E. S. Baker, J. Bertrand-Michel, J. A. Bowden, B. Brugger, S. R. Ellis, M. Fedorova, W. J. Griffiths, X. Han, J. Hartler, N. Hoffmann, J. P. Koelmel, H. C. Köfeler, T. W. Mitchell, V. B. O'Donnell, D. Saigusa, D. Schwudke, A. Shevchenko, C. Z. Ulmer, M. R. Wenk, M. Witting, D. Wolrab, Y. Xia, R. Ahrends, G. Liebisch, K. Ekroos, *Nat. Metab.* **2022**, *4*, 1086–1088.
[17] a) F. Tureček, *Mass Spectrom. Rev.* **2023**, *42*, 206–226; b) R. R. Julian, *J. Am. Soc. Mass Spectrom.* **2017**, *28*, 1823–1826.
[18] S. A. McLuckey, D. E. Goeringer, *J. Mass Spectrom.* **1997**, *32*, 461–474.
[19] J. Oomens, B. G. Sartakov, G. Meijer, G. von Helden, *Int. J. Mass Spectrom.* **2006**, *254*, 1–19.
[20] R. Antoine, J. Lemoine, P. Dugourd, *Mass Spectrom. Rev.* **2014**, *33*, 501–522.
[21] D. P. Little, J. P. Speir, M. W. Senko, P. B. O'Connor, F. W. McLafferty, *Anal. Chem.* **1994**, *66*, 2809–2815.
[22] H. J. Yoo, H. Liu, K. Håkansson, *Anal. Chem.* **2007**, *79*, 7858–7866.
[23] C. R. Raetz, C. M. Reynolds, M. S. Trent, R. E. Bishop, *Annu. Rev. Biochem.* **2007**, *76*, 295–329.
[24] J. A. Madsen, T. W. Cullen, M. S. Trent, J. S. Brodbelt, *Anal. Chem.* **2011**, *83*, 5107–5113.
[25] J. W. Jones, S. A. Shaffer, R. K. Ernst, D. R. Goodlett, F. Turecek, *Proc. Natl. Acad. Sci. USA* **2008**, *105*, 12742–12747.
[26] a) A. N. Kondakova, E. V. Vinogradov, Y. A. Knirel, B. Lindner, *Rapid Commun. Mass Spectrom.* **2005**, *19*, 2343–2349; b) A. Kondakov, B. Lindner, *Eur. J. Mass Spectrom.* **2005**, *11*, 535–546.
[27] N. Zehethofer, T. Scior, B. Lindner, *Anal. Bioanal. Chem.* **2010**, *398*, 2843–2851.
[28] F.-F. Hsu, J. Turk, *J. Am. Soc. Mass Spectrom.* **2000**, *11*, 986–999.
[29] M. Gilleron, B. Lindner, G. Puzo, *Anal. Chem.* **2006**, *78*, 8543–8548.
[30] M. A. McFarland, A. G. Marshall, C. L. Hendrickson, C. L. Nilsson, P. Fredman, J. E. Mansson, *J. Am. Soc. Mass Spectrom.* **2005**, *16*, 752–762.
[31] L. Cui, M. A. Isbell, Y. Chawengsub, J. R. Falck, W. B. Campbell, K. Nithipatikom, *J. Am. Soc. Mass Spectrom.* **2008**, *19*, 569–585.
[32] V. A. Mikhailov, I. Liko, T. H. Mize, M. F. Bush, J. L. Benesch, C. V. Robinson, *Anal. Chem.* **2016**, *88*, 7060–7067.
[33] N. P. Barrera, N. Di Bartolo, P. J. Booth, C. V. Robinson, *Science* **2008**, *321*, 243–246.

[34] A. S. Hauser, M. M. Attwood, M. Rask-Andersen, H. B. Schioth, D. E. Gloriam, *Nat. Rev. Drug Discovery* **2017**, *16*, 829–842.
[35] R. Baccouch, E. Rascol, K. Stoklosa, I. D. Alves, *Biophys. Chem.* **2022**, *285*, 106794.
[36] W. D. Bowers, S. S. Delbert, R. L. Hunter, R. T. McIver, *J. Am. Chem. Soc.* **1984**, *106*, 7288–7289.
[37] M. S. Blevins, D. R. Klein, J. S. Brodbelt, *Anal. Chem.* **2019**, *91*, 6820–6828.
[38] D. R. Klein, J. S. Brodbelt, *Anal. Chem.* **2017**, *89*, 1516–1522.
[39] L. A. Macias, K. Y. Garza, C. L. Feider, L. S. Eberlin, J. S. Brodbelt, *J. Am. Chem. Soc.* **2021**, *143*, 14622–14634.
[40] S. W. J. Shields, J. D. Sanders, J. S. Brodbelt, *Anal. Chem.* **2022**, *94*, 11352–11359.
[41] P. E. Williams, D. R. Klein, S. M. Greer, J. S. Brodbelt, *J. Am. Chem. Soc.* **2017**, *139*, 15681–15690.
[42] D. R. Klein, C. L. Feider, K. Y. Garza, J. Q. Lin, L. S. Eberlin, J. S. Brodbelt, *Anal. Chem.* **2018**, *90*, 10100–10104.
[43] C. L. Feider, L. A. Macias, J. S. Brodbelt, L. S. Eberlin, *Anal. Chem.* **2020**, *92*, 8386–8395.
[44] M. Fang, Y. Rustam, M. Palmieri, O. M. Sieber, G. E. Reid, *Anal. Bioanal. Chem.* **2020**, *412*, 2339–2351.
[45] D. R. Klein, M. S. Blevins, L. A. Macias, M. V. Douglass, M. S. Trent, J. S. Brodbelt, *Anal. Chem.* **2020**, *92*, 5986–5993.
[46] M. S. Blevins, V. K. James, C. M. Herrera, A. B. Purcell, M. S. Trent, J. S. Brodbelt, *Anal. Chem.* **2020**, *92*, 9146–9155.
[47] a) L. A. Macias, C. L. Feider, L. S. Eberlin, J. S. Brodbelt, *Anal. Chem.* **2019**, *91*, 12509–12516; b) L. A. Macias, J. S. Brodbelt, *Anal. Chem.* **2022**, *94*, 3268–3277.
[48] a) J. V. Hankins, J. A. Madsen, D. K. Giles, B. M. Childers, K. E. Klose, J. S. Brodbelt, M. S. Trent, *Mol. Microbiol.* **2011**, *81*, 1313–1329; b) J. V. Hankins, J. A. Madsen, D. K. Giles, J. S. Brodbelt, M. S. Trent, *Proc. Natl. Acad. Sci. USA* **2012**, *109*, 8722–8727; c) E. M. Nowicki, J. P. O'Brien, J. S. Brodbelt, M. S. Trent, *Mol. Microbiol.* **2014**, *94*, 728–741; d) E. M. Nowicki, J. P. O'Brien, J. S. Brodbelt, M. S. Trent, *Mol. Microbiol.* **2015**, *97*, 166–178; e) J. M. Boll, A. T. Tucker, D. R. Klein, A. M. Beltran, J. S. Brodbelt, B. W. Davies, M. S. Trent, *mBio* **2015**, *6*, e00478–00415; f) C. Bure, C. Le Senechal, L. Macias, C. Tokarski, S. Vilain, J. S. Brodbelt, *Anal. Chem.* **2021**, *93*, 4255–4262; g) J. P. O'Brien, B. D. Needham, J. C. Henderson, E. M. Nowicki, M. S. Trent, J. S. Brodbelt, *Anal. Chem.* **2014**, *86*, 2138–2145; h) L. J. Morrison, W. R. Parker, D. D. Holden, J. C. Henderson, J. M. Boll, M. S. Trent, J. S. Brodbelt, *Anal. Chem.* **2016**, *88*, 1812–1820; i) C. M. Crittenden, C. M. Herrera, P. E. Williams, D. P. Ricci, L. R. Swem, M. S. Trent, J. S. Brodbelt, *Analyst* **2018**, *143*, 3091–3099; j) C. M. Crittenden, L. D. Akin, L. J. Morrison, M. S. Trent, J. S. Brodbelt, *J. Am. Soc. Mass Spectrom.* **2017**, *28*, 1118–1126; k) J. P. O'Brien, B. D. Needham, D. B. Brown, M. S. Trent, J. S. Brodbelt, *Chem. Sci.* **2014**, *5*, 4291–4301; l) D. R. Klein, D. D. Holden, J. S. Brodbelt, *Anal. Chem.* **2016**, *88*, 1044–1051; m) D. R. Klein, M. J. Powers, M. S. Trent, J. S. Brodbelt, *Anal. Chem.* **2019**, *91*, 9608–9615; n) B. L. Oyler, M. M. Khan, D. F. Smith, E. M. Harberts, D. P. A. Kilgour, R. K. Ernst, A. S. Cross, D. R. Goodlett, *J. Am. Soc. Mass Spectrom.* **2018**, *29*, 1221–1229.
[49] J. P. O'Brien, J. S. Brodbelt, *Anal. Chem.* **2013**, *85*, 10399–10407.
[50] J. V. Hankins, J. A. Madsen, B. D. Needham, J. S. Brodbelt, M. S. Trent, in *Bacterial Cell Surfaces*, Springer, **2013**, pp. 239–258.
[51] E. Ryan, C. Q. N. Nguyen, C. Shiea, G. E. Reid, *J. Am. Soc. Mass Spectrom.* **2017**, *28*, 1406–1419.
[52] M. S. Blevins, S. W. J. Shields, W. Cui, W. Fallatah, A. B. Moser, N. E. Braverman, J. S. Brodbelt, *Anal. Chem.* **2022**, *94*, 12621–12629.
[53] E. W. Buenger, G. E. Reid, *Eur. J. Mass Spectrom.* **2020**, *26*, 311–323.
[54] M. M. Yore, I. Syed, P. M. Moraes-Vieira, T. Zhang, M. A. Herman, E. A. Homan, R. T. Patel, J. Lee, S. Chen, O. D. Peroni, A. S. Dhaneshwar, A. Hammarstedt, U. Smith, T. E. McGraw, A. Saghatelian, B. B. Kahn, *Cell* **2014**, *159*, 318–332.
[55] H. West, G. E. Reid, *Anal. Chim. Acta* **2021**, *1141*, 100–109.
[56] S. Becher, B. Spengler, S. Heiles, *Eur. J. Mass Spectrom.* **2018**, *24*, 54–65.
[57] S. Becher, P. Esch, S. Heiles, *Anal. Chem.* **2018**, *90*, 11486–11494.
[58] A. Devakumar, D. K. O'Dell, J. M. Walker, J. P. Reilly, *J. Am. Soc. Mass Spectrom.* **2008**, *19*, 14–26.
[59] a) S. M. Zucker, S. Lee, N. Webber, S. J. Valentine, J. P. Reilly, D. E. Clemmer, *J. Am. Soc. Mass Spectrom.* **2011**, *22*, 1477–1485; b) S. Warnke, C. Baldauf, M. T. Bowers, K. Pagel, G. von Helden, *J. Am. Chem. Soc.* **2014**, *136*, 10308–10314; c) A. L. Simon, F. Chirot, C. M. Choi, C. Clavier, M. Barbaire, J. Maurelli, X. Dagany, L. MacAleese, P. Dugourd, *Rev. Sci. Instrum.* **2015**, *86*, 094101; d) B. Bellina, J. M. Brown, J. Ujma, P. Murray, K. Giles, M. Morris, I. Compagnon, P. E. Barran, *Analyst* **2014**, *139*, 6348–6351; e) J. D. Sanders, S. W. Shields, E. E. Escobar, M. B. Lanzillotti, J. P. Butalewicz, V. K. James, M. S. Blevins, S. N. Sipe, J. S. Brodbelt, *Anal. Chem.* **2022**, *94*, 4252–4259.
[60] H. Borsdorf, G. A. Eiceman, *Appl. Spectrosc. Rev.* **2006**, *41*, 323–375.
[61] J. E. Kyle, X. Zhang, K. K. Weitz, M. E. Monroe, Y. M. Ibrahim, R. J. Moore, J. Cha, X. Sun, E. S. Lovelace, J. Wagoner, S. J. Polyak, T. O. Metz, S. K. Dey, R. D. Smith, K. E. Burnum-Johnson, E. S. Baker, *Analyst* **2016**, *141*, 1649–1659.
[62] T. Ly, R. R. Julian, *J. Am. Chem. Soc.* **2008**, *130*, 351–358.
[63] Q. Lin, P. Li, R. Jian, Y. Xia, *J. Am. Soc. Mass Spectrom.* **2022**, *33*, 714–721.
[64] a) H. T. Pham, T. Ly, A. J. Trevitt, T. W. Mitchell, S. J. Blanksby, *Anal. Chem.* **2012**, *84*, 7525–7532; b) H. T. Pham, A. J. Trevitt, T. W. Mitchell, S. J. Blanksby, *Rapid Commun. Mass Spectrom.* **2013**, *27*, 805–815.
[65] H. T. Pham, M. B. Prendergast, C. W. Dunstan, A. J. Trevitt, T. W. Mitchell, R. R. Julian, S. J. Blanksby, *Int. J. Mass Spectrom.* **2015**, *390*, 170–177.
[66] S. Nie, H. T. Pham, S. J. Blanksby, G. E. Reid, *Eur. J. Mass Spectrom.* **2015**, *21*, 287–296.
[67] V. R. Narreddula, N. R. Boase, R. Ailuri, D. L. Marshall, B. L. J. Poad, M. J. Kelso, A. J. Trevitt, T. W. Mitchell, S. J. Blanksby, *Anal. Chem.* **2019**, *91*, 9901–9909.
[68] a) S. E. Hancock, R. Ailuri, D. L. Marshall, S. H. J. Brown, J. T. Saville, V. R. Narreddula, N. R. Boase, B. L. J. Poad, A. J. Trevitt, M. D. P. Willcox, M. J. Kelso, T. W. Mitchell, S. J. Blanksby, *J. Lipid Res.* **2018**, *59*, 1510–1518; b) V. R. Narreddula, P. Sadowski, N. R. B. Boase, D. L. Marshall, B. L. J. Poad, A. J. Trevitt, T. W. Mitchell, S. J. Blanksby, *Rapid Commun. Mass Spectrom.* **2020**, *34*, e8741.
[69] V. R. Narreddula, B. I. McKinnon, S. J. P. Marlton, D. L. Marshall, N. R. B. Boase, B. L. J. Poad, A. J. Trevitt, T. W. Mitchell, S. J. Blanksby, *Analyst* **2021**, *146*, 156–169.
[70] H. T. Pham, R. R. Julian, *Anal. Chem.* **2014**, *86*, 3020–3027.
[71] H. T. Pham, R. R. Julian, *Int. J. Mass Spectrom.* **2014**, *370*, 58–65.
[72] H. T. Pham, R. R. Julian, *Analyst* **2016**, *141*, 1273–1278.
[73] a) H.-F. Li, J. Zhao, W. Cao, W. Zhang, Y. Xia, Z. Ouyang, *Research* **2022**, *2022*, 1–12; b) F. Wäldchen, S. Becher, P. Esch, M. Kompauer, S. Heiles, *Analyst* **2017**, *142*, 4744–4755.
[74] X. Ma, Y. Xia, *Angew. Chem. Int. Ed.* **2014**, *53*, 2592–2596; *Angew. Chem.* **2014**, *126*, 2630–2634.
[75] A. M. Rijs, J. Oomens, *Top. Curr. Chem.* **2015**, *364*, 1–42.
[76] E. Saparbaev, R. Yamaletdinov, O. V. Boyarkin, *Anal. Chem.* **2021**, *93*, 12822–12826.
[77] A. Pereverzev, J. Roithova, *J. Mass Spectrom.* **2022**, *57*, e4826.
[78] V. Kopysov, A. Makarov, O. V. Boyarkin, *Anal. Chem.* **2015**, *87*, 4607–4611.
[79] R. Antoine, P. Dugourd, in *Laser Photodissociation and Spectroscopy of Mass-separated Biomolecular Ions*, Springer, Cham, **2013**, pp. 93–116.
[80] E. Saparbaev, V. Kopysov, R. Yamaletdinov, A. Y. Pereverzev, O. V. Boyarkin, *Angew. Chem. Int. Ed.* **2019**, *58*, 7346–7350; *Angew. Chem.* **2019**, *131*, 7424–7428.
[81] E. Saparbaev, V. Kopysov, V. Aladinskaia, V. Ferrieres, L. Legentil, O. V. Boyarkin, *Anal. Chem.* **2020**, *92*, 14624–14632.
[82] A. A. Lobas, E. M. Solovyeva, E. Saparbaev, M. V. Gorshkov, O. V. Boyarkin, *Talanta* **2021**, *232*, 122412.
[83] V. Kopysov, A. Makarov, O. V. Boyarkin, *Anal. Chem.* **2017**, *89*, 544–547.
[84] E. Saparbaev, A. Zviagin, O. V. Boyarkin, *Anal. Chem.* **2022**, *94*, 9514–9518.
[85] B. D. Adamson, N. J. Coughlan, P. B. Markworth, R. E. Continetti, E. J. Bieske, *Rev. Sci. Instrum.* **2014**, *85*, 123109.
[86] a) N. J. Coughlan, K. J. Catani, B. D. Adamson, U. Wille, E. J. Bieske, *J. Chem. Phys.* **2014**, *140*, 164307; b) N. J. Coughlan, M. S. Scholz, C. S. Hansen, A. J. Trevitt, B. D. Adamson, E. J. Bieske, *J. Am. Soc. Mass Spectrom.* **2016**, *27*, 1483–1490; c) N. J. Coughlan, B. D. Adamson, K. J. Catani, U. Wille, E. J. Bieske, *J. Phys. Chem. Lett.* **2014**, *5*, 3195–3199; d) J. N. Bull, C. W. West, C. S. Anstoter, G. da Silva, E. J. Bieske, J. R. R. Verlet, *Phys. Chem. Chem. Phys.* **2019**, *21*, 10567–10579.
[87] R. W. Schoenlein, L. A. Peteanu, R. A. Mathies, C. V. Shank, *Science* **1991**, *254*, 412–415.
[88] a) G. Papadopoulos, A. Svendsen, O. V. Boyarkin, T. R. Rizzo, *Faraday Discuss.* **2011**, *150*, 243–255; b) S. J. P. Marlton, B. I. McKinnon, B. Ucur, A. T. Maccarone, W. A. Donald, S. J. Blanksby, A. J. Trevitt, *Faraday Discuss.* **2019**, *217*, 453–475; c) N. J. A. Coughlan, P. J. J. Carr, S. C. Walker, C. Zhou, M. Guna, J. L. Campbell, W. S. Hopkins, *J. Am. Soc. Mass Spectrom.* **2020**, *31*, 405–410.

[89] A. T. Kirk, A. Bohnhorst, C. R. Raddatz, M. Allers, S. Zimmermann, *Anal. Bioanal. Chem.* **2019**, *411*, 6229–6246.
[90] R. J. Lipert, S. D. Colson, *J. Phys. Chem.* **1989**, *93*, 3894–3896.
[91] a) C. M. Choi, D. H. Choi, J. Heo, N. J. Kim, S. K. Kim, *Angew. Chem. Int. Ed.* **2012**, *51*, 7297–7300; *Angew. Chem.* **2012**, *124*, 7409–7412; b) G. Feraud, C. Dedonder, C. Jouvet, Y. Inokuchi, T. Haino, R. Sekiya, T. Ebata, *J. Phys. Chem. Lett.* **2014**, *5*, 1236–1240.
[92] a) F. Morishima, Y. Inokuchi, T. Ebata, *J. Phys. Chem. A* **2012**, *116*, 8201–8208; b) F. Morishima, Y. Inokuchi, T. Ebata, *J. Phys. Chem. A* **2013**, *117*, 13543–13555.
[93] a) J. Jasik, R. Navratil, I. Nemec, J. Roithova, *J. Phys. Chem. A* **2015**, *119*, 12648–12655; b) R. Navrátil, J. Jašík, J. Roithová, *J. Mol. Spectrosc.* **2017**, *332*, 52–58; c) M. Srnec, R. Navratil, E. Andris, J. Jasik, J. Roithova, *Angew. Chem. Int. Ed.* **2018**, *57*, 17053–17057; *Angew. Chem.* **2018**, *130*, 17299–17303.
[94] J. P. Toennies, A. F. Vilesov, K. B. Whaley, *Phys. Today* **2001**, *54*, 31–37.
[95] S. Albertini, E. Gruber, F. Zappa, S. Krasnokutski, F. Laimer, P. Scheier, *Mass Spectrom. Rev.* **2022**, *41*, 529–567.
[96] N. B. Brauer, S. Smolarek, X. Zhang, W. J. Buma, M. Drabbels, *J. Phys. Chem. Lett.* **2011**, *2*, 1563–1566.
[97] a) F. Bierau, P. Kupser, G. Meijer, G. von Helden, *Phys. Rev. Lett.* **2010**, *105*, 133402; b) F. Filsinger, D. S. Ahn, G. Meijer, G. von Helden, *Phys. Chem. Chem. Phys.* **2012**, *14*, 13370–13377.
[98] a) S. Daly, F. Rosu, V. Gabelica, *Science* **2020**, *368*, 1465–1468; b) H. J. Eun, A. Min, C. W. Jeon, I. T. Yoo, J. Heo, N. J. Kim, *J. Phys. Chem. Lett.* **2020**, *11*, 4367–4371.
[99] a) S. Hanashima, Y. Yano, M. Murata, *Chirality* **2020**, *32*, 282–298; b) T. O. Eichmann, A. Lass, *Cell. Mol. Life Sci.* **2015**, *72*, 3931–3952.
[100] A. P. Cismesia, M. R. Bell, L. F. Tesler, M. Alves, N. C. Polfer, *Analyst* **2018**, *143*, 1615–1623.
[101] J. P. Toennies, A. F. Vilesov, *Angew. Chem. Int. Ed.* **2004**, *43*, 2622–2648; *Angew. Chem.* **2004**, *116*, 2674–2702.
[102] G. Berden, M. Derksen, K. J. Houthuijs, J. Martens, J. Oomens, *Int. J. Mass Spectrom.* **2019**, *443*, 1–8.
[103] R. E. van Outersterp, J. Martens, A. Peremans, L. Lamard, F. Cuyckens, J. Oomens, G. Berden, *Analyst* **2021**, *146*, 7218–7229.
[104] D. Oepts, A. F. G. van der Meer, P. W. van Amersfoort, *Infrared Phys. Technol.* **1995**, *36*, 297–308.
[105] R. Prazeres, J. M. Berset, R. Chaput, F. Glotin, D. A. Jaroszynski, J. M. Ortega, *Nucl. Instrum. Methods Phys. Res. Sect. B* **1994**, *89*, 54–59.
[106] W. Schöllkopf, S. Gewinner, H. Junkes, A. Paarmann, G. von Helden, H. Bluem, A. M. M. Todd, *Proc. SPIE* **2015**, *9512*, 95121 L.
[107] O. Yeni, B. Schindler, B. Moge, I. Compagnon, *Analyst* **2022**, *147*, 312–317.
[108] M. J. Carlo, A. L. Patrick, *J. Mass Spectrom. Adv. Clin. Lab.* **2022**, *23*, 14–25.
[109] a) J. Martens, G. Berden, H. Bentlage, K. L. M. Coene, U. F. Engelke, D. Wishart, M. van Scherpenzeel, L. A. J. Kluijtmans, R. A. Wevers, J. Oomens, *J. Inherited Metab. Dis.* **2018**, *41*, 367–377; b) R. E. van Outersterp, K. J. Houthuijs, G. Berden, U. F. Engelke, L. A. J. Kluijtmans, R. A. Wevers, K. L. M. Coene, J. Oomens, J. Martens, *Int. J. Mass Spectrom.* **2019**, *443*, 77–85; c) E. Q. Walhout, S. E. Dorn, J. Martens, G. Berden, J. Oomens, P. H. Cheong, J. H. Kroll, R. E. O'Brien, *Environ. Sci. Technol.* **2019**, *53*, 7604–7612.
[110] a) R. E. van Outersterp, J. Martens, G. Berden, V. Koppen, F. Cuyckens, J. Oomens, *Analyst* **2020**, *145*, 6162–6170; b) R. F. Kranenburg, F. van Geenen, G. Berden, J. Oomens, J. Martens, A. C. van Asten, *Anal. Chem.* **2020**, *92*, 7282–7288.
[111] R. Han, R. Ketkaew, S. Luber, *J. Phys. Chem. A* **2022**, *126*, 801–812.
[112] J. Martens, V. Koppen, G. Berden, F. Cuyckens, J. Oomens, *Anal. Chem.* **2017**, *89*, 4359–4362.
[113] R. E. van Outersterp, U. F. H. Engelke, J. Merx, G. Berden, M. Paul, T. Thomulka, A. Berkessel, M. Huigen, L. A. J. Kluijtmans, J. Mecinovic, F. Rutjes, C. D. M. van Karnebeek, R. A. Wevers, T. J. Boltje, K. L. M. Coene, J. Martens, J. Oomens, *Anal. Chem.* **2021**, *93*, 15340–15348.
[114] B. Schindler, G. Laloy-Borgna, L. Barnes, A. R. Allouche, E. Bouju, V. Dugas, C. Demesmay, I. Compagnon, *Anal. Chem.* **2018**, *90*, 11741–11745.
[115] S. Warnke, A. Ben Faleh, T. R. Rizzo, *ACS Meas. Sci. Au* **2021**, *1*, 157–164.
[116] F. van Geenen, R. F. Kranenburg, A. C. van Asten, J. Martens, J. Oomens, G. Berden, *Anal. Chem.* **2021**, *93*, 2687–2693.
[117] S. Warnke, J. Seo, J. Boschmans, F. Sobott, J. H. Scrivens, C. Bleiholder, M. T. Bowers, S. Gewinner, W. Schöllkopf, K. Pagel, G. von Helden, *J. Am. Chem. Soc.* **2015**, *137*, 4236–4242.
[118] O. Hernandez, S. Isenberg, V. Steinmetz, G. L. Glish, P. Maitre, *J. Phys. Chem. A* **2015**, *119*, 6057–6064.
[119] B. Schindler, A. D. Depland, G. Renois-Predelus, G. Karras, B. Concina, G. Celep, J. Maurelli, V. Loriot, E. Constant, R. Bredy, C. Bordas, F. Lépine, I. Compagnon, *Int. J. Ion Mobility Spectrom.* **2017**, *20*, 119–124.
[120] M. Thevis, S. Beuck, S. Hoppner, A. Thomas, J. Held, M. Schafer, J. Oomens, W. Schanzer, *J. Am. Soc. Mass Spectrom.* **2012**, *23*, 537–546.
[121] S. Becher, G. Berden, J. Martens, J. Oomens, S. Heiles, *J. Am. Soc. Mass Spectrom.* **2021**, *32*, 2874–2884.
[122] M. Hermansson, K. Hokynar, P. Somerharju, *Prog. Lipid Res.* **2011**, *50*, 240–257.
[123] C. Kirschbaum, K. Greis, L. Polewski, S. Gewinner, W. Schöllkopf, G. Meijer, G. von Helden, K. Pagel, *J. Am. Chem. Soc.* **2021**, *143*, 14827–14834.
[124] O. V. Boyarkin, S. R. Mercier, A. Kamariotis, T. R. Rizzo, *J. Am. Chem. Soc.* **2006**, *128*, 2816–2817.
[125] a) A. P. Cismesia, L. F. Tesler, M. R. Bell, L. S. Bailey, N. C. Polfer, *J. Mass Spectrom.* **2017**, *52*, 720–727; b) L. F. Tesler, A. P. Cismesia, M. R. Bell, L. S. Bailey, N. C. Polfer, *J. Am. Soc. Mass Spectrom.* **2018**, *29*, 2115–2124.
[126] M. Z. Kamrath, E. Garand, P. A. Jordan, C. M. Leavitt, A. B. Wolk, M. J. Van Stipdonk, S. J. Miller, M. A. Johnson, *J. Am. Chem. Soc.* **2011**, *133*, 6440–6448.
[127] M. Z. Kamrath, R. A. Relph, T. L. Guasco, C. M. Leavitt, M. A. Johnson, *Int. J. Mass Spectrom.* **2011**, *300*, 91–98.
[128] O. Gorlova, S. M. Colvin, A. Brathwaite, F. S. Menges, S. M. Craig, S. J. Miller, M. A. Johnson, *J. Am. Soc. Mass Spectrom.* **2017**, *28*, 2414–2422.
[129] a) B. M. Elliott, R. A. Relph, J. R. Roscioli, J. C. Bopp, G. H. Gardenier, T. L. Guasco, M. A. Johnson, *J. Chem. Phys.* **2008**, *129*, 094303; b) C. M. Leavitt, A. B. Wolk, J. A. Fournier, M. Z. Kamrath, E. Garand, M. J. Van Stipdonk, M. A. Johnson, *J. Phys. Chem. Lett.* **2012**, *3*, 1099–1105.
[130] J. M. Voss, S. J. Kregel, K. C. Fischer, E. Garand, *J. Am. Soc. Mass Spectrom.* **2018**, *29*, 42–50.
[131] V. Scutelnic, T. R. Rizzo, *J. Phys. Chem. A* **2019**, *123*, 2815–2819.
[132] S. Warnke, A. Ben Faleh, R. P. Pellegrinelli, N. Yalovenko, T. R. Rizzo, *Faraday Discuss.* **2019**, *217*, 114–125.
[133] C. Kirschbaum, K. Greis, E. Mucha, L. Kain, S. Deng, A. Zappe, S. Gewinner, W. Schöllkopf, G. von Helden, G. Meijer, P. B. Savage, M. Marianski, L. Teyton, K. Pagel, *Nat. Commun.* **2021**, *12*, 1201.
[134] a) M. S. de Vries, P. Hobza, *Annu. Rev. Phys. Chem.* **2007**, *58*, 585–612; b) E. C. Stanca-Kaposta, J. P. Simons, in *Handbook of High-resolution Spectroscopy, Vol. 3* (Eds.: M. Quack, F. Merkt), Wiley, New York, **2011**, pp. 1911–1941.
[135] A. Ben Faleh, S. Warnke, T. R. Rizzo, *Anal. Chem.* **2019**, *91*, 4876–4882.
[136] I. K. Webb, S. V. Garimella, A. V. Tolmachev, T. C. Chen, X. Zhang, R. V. Norheim, S. A. Prost, B. LaMarche, G. A. Anderson, Y. M. Ibrahim, R. D. Smith, *Anal. Chem.* **2014**, *86*, 9169–9176.
[137] a) R. Wojcik, I. K. Webb, L. Deng, S. V. Garimella, S. A. Prost, Y. M. Ibrahim, E. S. Baker, R. D. Smith, *Int. J. Mol. Sci.* **2017**, *18*, 183; b) J. C. May, K. L. Leaptrot, B. S. Rose, K. L. W. Moser, L. Deng, L. Maxon, D. DeBord, J. A. McLean, *J. Am. Soc. Mass Spectrom.* **2021**, *32*, 1126–1137.
[138] B. S. Rose, J. C. May, A. R. Reardon, J. A. McLean, *J. Am. Soc. Mass Spectrom.* **2022**, *33*, 1229–1237.
[139] C. Masellis, N. Khanal, M. Z. Kamrath, D. E. Clemmer, T. R. Rizzo, *J. Am. Soc. Mass Spectrom.* **2017**, *28*, 2217–2222.
[140] R. P. Pellegrinelli, L. Yue, E. Carrascosa, A. Ben Faleh, S. Warnke, P. Bansal, T. R. Rizzo, *J. Am. Soc. Mass Spectrom.* **2022**, *33*, 859–864.
[141] V. Yatsyna, A. H. Abikhodr, A. Ben Faleh, S. Warnke, T. R. Rizzo, *Anal. Chem.* **2022**, *94*, 2912–2917.
[142] D. Verma, R. M. P. Tanyag, S. M. O. O'Connell, A. F. Vilesov, *Adv. Phys.: X* **2019**, *4*, 1553569.
[143] S. Smolarek, N. B. Brauer, W. J. Buma, M. Drabbels, *J. Am. Chem. Soc.* **2010**, *132*, 14086–14091.
[144] A. I. González Flórez, D. S. Ahn, S. Gewinner, W. Schöllkopf, G. von Helden, *Phys. Chem. Chem. Phys.* **2015**, *17*, 21902–21911.
[145] D. Mani, T. Fischer, R. Schwan, A. Dey, B. Redlich, A. F. G. Van der Meer, G. Schwaab, M. Havenith, *RSC Adv.* **2017**, *7*, 54318–54325.
[146] F.-F. Hsu, J. Turk, *J. Am. Soc. Mass Spectrom.* **2003**, *14*, 352–363.
[147] C. Kirschbaum, K. Greis, S. Gewinner, W. Schöllkopf, G. Meijer, G. von Helden, K. Pagel, *Anal. Bioanal. Chem.* **2022**, *414*, 5275–5285.
[148] C. Kirschbaum, E. M. Saied, K. Greis, E. Mucha, S. Gewinner, W. Schöllkopf, G. Meijer, G. von Helden, B. L. J. Poad, S. J. Blanksby, C. Arenz, K. Pagel, *Angew. Chem. Int. Ed.* **2020**, *59*, 13638–13642; *Angew. Chem.* **2020**, *132*, 13740–13744.

[149] C. Kirschbaum, K. Greis, M. Lettow, S. Gewinner, W. Schöllkopf, G. Meijer, G. von Helden, K. Pagel, *Anal. Bioanal. Chem.* **2021**, *413*, 3643–3653.
[150] B. L. J. Poad, A. T. Maccarone, H. Yu, T. W. Mitchell, E. M. Saied, C. Arenz, T. Hornemann, J. N. Bull, E. J. Bieske, S. J. Blanksby, *Anal. Chem.* **2018**, *90*, 5343–5351.
[151] A. H. Abikhodr, V. Yatsyna, A. Ben Faleh, S. Warnke, T. R. Rizzo, *Anal. Chem.* **2021**, *93*, 14730–14736.
[152] D. D. Holden, A. Makarov, J. C. Schwartz, J. D. Sanders, E. Zhuk, J. S. Brodbelt, *Angew. Chem. Int. Ed.* **2016**, *55*, 12417–12421; *Angew. Chem.* **2016**, *128*, 12605–12609.
[153] A. Giuliani, J. P. Williams, M. R. Green, *Anal. Chem.* **2018**, *90*, 7176–7180.
[154] S. Ickert, S. Beck, M. W. Linscheid, J. Riedel, *J. Am. Soc. Mass Spectrom.* **2019**, *30*, 2114–2122.
[155] A. Godard, *C. R. Phys.* **2007**, *8*, 1100–1128.
[156] P. Figueiredo, M. Suttinger, R. Go, E. Tsvid, C. K. N. Patel, A. Lyakh, *Appl. Opt.* **2017**, *56*, H15-H23.
[157] S. B. Mirov, I. S. Moskalev, S. Vasilyev, V. Smolski, V. V. Fedorov, D. Martyshkin, J. Peppers, M. Mirov, A. Dergachev, V. Gapontsev, *IEEE J. Sel. Top. Quantum Electron.* **2018**, *24*, 1–29.

Manuscript received: November 15, 2022
Revised manuscript received: December 13, 2022
Accepted manuscript online: December 13, 2022
Version of record online: December 30, 2022